TITLE:

Targeting nuclear pore protein, NUP210, reduces metastasis through heterochromatin-mediated silencing of mechanosensitive genes

AUTHORS:

Ruhul Amin[1], Anjali Shukla[1], Jacqueline Jufen Zhu[2], Sohyoung Kim[3], Ping Wang[2], Simon Zhongyuan Tian[2], Steven D. Cappell[1], Sandra Burkett[4], Huaitian Liu[1,5], Maxwell P. Lee[1,5], Andy D. Tran[1,6], Michael J. Kruhlak[1,6], Gordon L. Hager[3], Yijun Ruan[2], Kent W. Hunter[1,*]

AFFILIATIONS:

[1]Laboratory of Cancer Biology and Genetics, Center for Cancer Research, National Cancer Institute, National Institutes of Health, Bethesda, MD 20892, USA

[2]The Jackson Laboratory for Genomic Medicine, Farmington, CT 06030, USA

[3]Laboratory of Receptor Biology and Gene Expression, Center for Cancer Research, National Cancer Institute, National Institutes of Health, Bethesda, MD 20892, USA

[4]Molecular Cytogenetics Core Facility, Center for Cancer Research, National Cancer Institute, National Institutes of Health, Frederick, MD 21702, USA

[5]High-Dimension Data Analysis Group, Laboratory of Cancer Biology and Genetics, Center for Cancer Research, National Cancer Institute, National Institutes of Health, Bethesda, MD 20892, USA

[6]Confocal Microscopy Core Facility, Center for Cancer Research, National Cancer Institute, National Institutes of Health, Bethesda, MD 20892, USA

***Correspondence:** hunterk@mail.nih.gov

Abstract:

Mechanical signals from the extracellular microenvironment have been implicated in tumor and metastatic progression. It remains unclear how these mechanical signals are transmitted to the cell nucleus to regulate gene expression in metastasis. In an attempt to characterize metastasis-associated polymorphisms in the non-coding regulatory regions of the genome, we identified nucleoporin *NUP210* as a metastasis susceptibility gene for human estrogen receptor positive (ER+) breast cancer and a cellular mechanosensor. Polymorphisms in the mouse *Nup210* promoter affect *Nup210* transcription via alteration of CTCF binding. Depletion of *Nup210* reduces lung metastasis in mouse models of breast cancer. Mechanistically, NUP210 interacts with histone H3.1/H3.2 at the nuclear periphery and prevents its heterochromatin (H3K27me3) modification to regulate mechanosensitive, metastasis- promoting gene expression. Upon *Nup210* knockout, these mechanosensitive genes are differentially repositioned and become repressed due to heterochromatinization. As a result, *Nup210* depletion decreases mechanotransduction and focal adhesion *in vitro* and circulating tumor cells *in vivo*. Our study provides a new insight into the role of nuclear pore protein in cellular mechanosensation and metastasis.

INTRODUCTION:

The majority of cancer-related mortality is due to distant organ metastasis, a process in which cancer cells must leave the primary tumor, intravasate into the surrounding endothelium, evade immunosurveillance in the circulation, travel to a distant site, extravasate, and colonize the secondary organ[1-3]. Due to the need to successfully complete each of these steps, metastasis is a highly inefficient process. To complete the whole metastatic cascade, cancer cells employ multiple genetic and epigenetic mechanisms. Because of the limited understanding of these mechanisms, it is difficult to target these aggressive cancer cells, even with the improved therapeutic strategies[4]. Hence, a more detailed understanding of the mechanisms by which cancer cells gain metastatic potential is crucial to ultimately improve patient outcomes.

With the advent of large-scale genome sequencing technology, remarkable progress has been made to characterize the genetic alterations in primary tumors[5]. In more recent years, an increased focus on the genomics of metastasis has emerged[6-9]. Such studies have suggested that a metastatic tumor clone may arise from the combined effect of certain genetic and epigenetic changes within primary tumor. These genetic changes include somatic mutation, copy number variation, loss of heterozygosity, and allelic imbalance. Epigenetic changes such as DNA methylation, histone modification, and chromatin remodeling can also affect gene expression in cancer[10]. Epigenetic silencing of tumor suppressor genes or activation of oncogenes has been implicated in cancer progression[11,12]. These genes can be silenced or activated through widespread alterations in chromatin accessibility due to the gain or loss of heterochromatin regions. Recent studies have shown increased chromatin accessibility[13] or disruption of large heterochromatin domains[14] during

metastatic progression from the primary tumor. However, the mechanisms by which chromatin boundary alterations affect metastasis remain largely unknown.

In addition to genetic and epigenetic changes, we previously demonstrated that germline polymorphism can affect metastatic outcome[15-17]. Since many of our polymorphic metastasis susceptibility genes were identified as chromatin-associated factors, we hypothesized that germline polymorphism can affect metastasis through alteration of the cancer cell's epigenome.To identify metastasis-associated polymorphisms in the non-coding regulatory regions of the genome, we performed genome-wide identification of polymorphic accessible chromatin regions in mouse models of metastasis and identified *Nup210*, a gene encoding a nuclear pore complex protein, as a potential metastasis susceptibility gene. Although nuclear pore complex proteins have recently been shown to be associated with several developmental disorders and cancers[18-21], their function in metastasis remains unexplored. Here, we established a nucleocytoplasmic transport-independent role of NUP210 in promoting lung metastasis in mouse models of breast cancer through alteration of mechanosensation, focal adhesion, and cell migration.

RESULTS:

Identification Nup210 as a candidate metastasis susceptibility gene

To identify accessible chromatin regions enriched during metastatic colonization, Benzonase-accessible chromatin (BACH) analysis was performed on the 4T07 and 4T1 isogenic cell lines derived from the spontaneous mammary tumor of BALB/cJ mice[22] (Fig. 1a; Shukla et al., in preparation). 67NR cells are tumorigenic when injected orthotopically into the mammary fat pad

of BALB/cJ mice, but they do not metastasize into distant organs. 4T07 cells produce primary tumors that disseminate to the lungs but only rarely form macroscopic metastasis. In contrast, 4T1 cells complete the metastatic process and form multiple macroscopic lesions in the lung upon orthotopic implantation[22]. We therefore hypothesized that differences in open chromatin between these two cell lines would be enriched for transcriptional control elements contributing to the dormant-to-proliferative switch during metastatic colonization. A total of 5303 BACH regions were unique to 4T1 cells and were therefore likely to be enriched in colonization-associated gene expression. Since the majority of inherited susceptibility is thought to result from polymorphisms in non-coding transcriptional control elements[23], the BACH regions were then intersected with known polymorphisms present in the Diversity Outbred (DO) panel[24], a highly polymorphic mouse genetic mapping panel generated from the random interbreeding of eight inbred mice strains. This identified a total of 1874 polymorphic BACH regions with the potential to alter gene transcriptional efficiency (Fig. 1a).

Preliminary analysis of the 1874 polymorphic BACH regions revealed that the majority (1477 out of 1874) did not overlap with gene promoters, defined here as regions extending 5 kb upstream and 1 kb downstream of the transcriptional start site. Since polymorphisms in enhancers are also thought to encode disease susceptibility, ChIA-PET (Chromatin Interaction Analysis through Paired-End Tag sequencing) analysis of the 4T1 cell line was performed and integrated with the BACH regions to identify gene promoters with single loops to putative polymorphic enhancers. This resulted in a total of 771 genes with potential colonization-associated polymorphic transcriptional control elements (Fig. 1a). As a final filtering step, the 771 genes were screened across a panel of tumors generated from a cross between the DO panel and a highly metastatic mammary tumor mouse model, MMTV-PyMT, to identify genes whose expression correlated with

distant metastasis-free survival (DMFS). Fifty-two of the 771 genes were significantly associated with DMFS in this tumor panel (Fig. 1a). Circos plot representation of these 52 genes revealed that some of them possess polymorphic promoters (Fig. 1b, red lines). In addition, many of these genes establish intra- and inter-chromosomal interaction in 4T1 cells (Fig. 1b, blue lines and light blue lines, respectively). To assess human relevance, the hazard ratios calculated for these 52 genes in the mouse data were used to generate a weighted gene signature that was subsequently screened on human breast cancer gene expression datasets. Significant stratification of DMFS in estrogen receptor-positive (ER+) breast cancer was observed in the human dataset (Fig. 1c), consistent with a significant association of these genes with human breast cancer progression and metastasis. NUP210, a nuclear pore protein, was selected for further validation due to the association of a number of metastasis susceptibility genes with the nuclear envelope. Also, our RNA-seq data on the isogenic 4T1 series of mouse cell lines revealed that the expression of *Nup210* was at the baseline level in the non-metastatic 67NR cell line, intermediate in the disseminating 4T07 cells but was sharply increased in the colonizing 4T1 cell line (Fig. 1d).

Polymorphisms in the Nup210 promoter affect CTCF binding and Nup210 transcription

Next, we explored whether genetic polymorphisms in the *Nup210* promoter affect *Nup210* expression. We focused on polymorphisms in the 510 bp mouse *Nup210* putative promoter region based on our BACH analysis on 4T07 and 4T1 cell lines (Fig. 1e). Within the 510 bp promoter region, six single nucleotide polymorphisms (SNPs) and one insertion/deletion (indel) were found among three different mouse strains in the Sanger Mouse Genome Repository[25] (Fig. 1f). Interestingly, Sanger sequencing analysis revealed that there was a 12 bp G-rich insertion in the

Nup210 promoter of the FVB/NJ strain that was located within the CTCF binding region in mouse mammary epithelial (ME) cells[26]. This particular region also showed enrichment for the H3K27Ac enhancer histone modification mark in mouse mammary luminal (ML) epithelial cells[27] and the H3K4me3 promoter mark in 4T1 cells (Fig. 1g). Occupancy of CTCF and H3K27Ac within the human *NUP210* promoter was also evident in publicly available ChIP-seq data from the MCF7 human breast cancer cell line, suggesting that the binding of CTCF to the *NUP210* promoter is evolutionarily conserved (Supplementary Fig. 1). As CTCFs have been shown to be enriched in the enhancer-promoter boundary or insulator element to regulate the gene expression[28,29], we hypothesized that polymorphic insertion in this region might affect CTCF binding and *Nup210* expression. Since 4T1 and 6DT1 metastatic mouse mammary cancer cell lines were derived from primary tumors from BALB/cJ and FVB/NJ mouse strains, respectively, we performed ChIP-qPCR analysis to compare the enrichment of CTCF and H3K27Ac in these two cell lines. Both CTCF and H3K27Ac marks were preferentially enriched in the *Nup210* promoter region of 4T1 cells as compared with 6DT1 cells (Fig. 1h). qRT-PCR analysis revealed that *Nup210* and *Ctcf* expression levels were significantly higher in 4T1 cells than in 6DT1 cells (Fig. 1i). Consistently, *Nup210* expression was significantly lower in the spleen of normal FVB/NJ mice than in BALB/cJ mice (Fig. 1j). However, *Ctcf* expression was not significantly different in the spleen, implying that the polymphism in *Nup210* might be responsible for the decreased expression in FVB/NJ strains despite the unaltered level of *Ctcf* (Fig. 1j). A promoter luciferase assay revealed that there was a moderate (~10%) reduction in luciferase activity for the FVB/NJ-derived *Nup210* promoter region as compared with the equivalent BALB/cJ promoter region (Fig. 1k). This result is consistent with the fact that CTCF mainly exerts its transcriptional activity through global alteration of chromatin architecture[30] and reporter assays using ectopically expressed plasmids

may not fully recapitulate CTCF activity in the native genomic context. To observe the direct effect of CTCF loss on *Nup210* transcription, we knocked down *Ctcf* in 4T1 cells and observed a marked reduction of *Nup210* both at the transcript (Fig. 1l) and protein level (Fig. 1m). Taken together, these results suggest that *Nup210* is a CTCF-regulated gene and polymorphisms in the *Nup210* promoter may affect CTCF binding in cancer cells.

NUP210 expression is associated with metastasis in human ER+ breast cancer patients

Examination of *NUP210* alterations in METABRIC[31] (Molecular Taxonomy of Breast Cancer International Consortium), a human breast cancer dataset, revealed that *NUP210* was amplified in 1.2 % of the cases and was associated with decreased overall survival (Fig. 2a). Examination of the *NUP210* mRNA expression level in the METABRIC dataset suggests that *NUP210* expression is significantly associated with reduced overall survival in ER+ breast cancer patients (Fig. 2b) but not in triple-negative (ER-/PR-/Her2-) patients (Fig. 2c). Consistently, survival analysis using an independent dataset from the Km-plotter database[32] revealed that *NUP210* expression is associated with poor distant metastasis-free survival in ER+ breast cancer patients (Fig. 2d) but not in triple-negative patients (Fig. 2e). An analysis of *NUP210* expression across PAM50 molecular subtypes from the METABRIC dataset suggests that *NUP210* expression is higher in luminal B and basal subtypes than in luminal A, Her2+, and claudin-low subtypes of breast cancer (Fig. 2f). Gene epression analysis from different metastatic sites of breast cancer revealed that *NUP210* expression is significantly higher in lung and liver metastases than lymph node metastases (Fig. 2g). Furthermore, analysis gene expression data from primary tumor and metastases suggested that *NUP210* expression is significantly higher in metastases than primary tumor of prostate cancer

(Fig. 2h) and melanoma (Fig. 2i). These data indicate that *NUP210* is associated with human cancer progression and further supports its potential role as a metastasis susceptibility gene.

Depletion of Nup210 in cancer cells decreases lung metastasis in mice

To test the function of *Nup210* in metastasis *in vivo*, we utilized mouse breast cancer orthotopic transplantation models that closely resemble human luminal breast cancers. Three different cell lines were utilized for this analysis: 4T1[22], 6DT1, derived from the mammary tumor of FVB/MMTV-MYC transgenic mouse, and MVT1, derived from the mammary tumor of FVB/MMTV-MYC/VEGF double transgenic mouse[33]. These cell lines form primary tumors and lung metastases within one month after mammary fat pad injection[34]. *Nup210* was knocked down through shRNA-mediated interference and knockdown was confirmed either through western blot or qRT-PCR (Fig. 3a, Supplementary Fig. 2a). Cell lines stably expressing two shRNAs, sh-Nup # 1 and # 4, were used for mouse injection as these showed consistent knockdown across cell lines. Primary tumors derived from *Nup210* knockdown cells showed variability in tumor weight, with decreased tumor weight in 4T1 cells but increased tumor weights for both 6DT1 and MVT1 cells (Fig. 3b, Supplementary Fig. 2b). However, knockdown of *Nup210* resulted in a decrease in pulmonary metastases for all three cell lines (Fig. 3c, Supplementary Fig. 2c), and this decrease was preserved after normalizing metastasis counts by tumor weight to account for the variability in primary tumor growth (Fig. 3d, Supplementary Fig. 2d). These results were therefore consistent with the association of *NUP210* with poor prognosis in patients with ER+ breast cancers.

To further validate the role of *Nup210* in metastatic progression, CRISPR/Cas9-mediated knockout of *Nup210* was performed in the 4T1 cell line (Fig. 3e). In agreement with the shRNA

result, CRISPR-mediated knockout of *Nup210* in two different clones, N9 and N13, dramatically diminished primary tumor weight and lung metastases (Fig. 3f-h). Since we observed differential effects of *Nup210* loss on primary tumor weight, we asked whether *Nup210* depletion affects cell proliferation. Cell cycle analysis on *Nup210* knockout 4T1 cells (Supplementary Fig. 3a, b) revealed that there was no consistent change in the distribution of cell population among cell cycle stages, suggesting that the effect of NUP210 loss on the primary tumor is independent of the intrinsic ability of NUP210 to regulate cell proliferation. Finally, 4T1 cells with stable overexpression of *Nup210* showed no difference in primary tumor weight (Fig. 3i, j). However, lung metastasis count was significantly increased by *Nup210* overexpression (Fig. 3k). Taken together, these results indicate that *Nup210* promotes lung metastasis in mouse models of luminal breast cancer.

Nup210 loss does not affect general nucleocytoplasmic protein transport but may affect RNA transport

The major function of the nuclear pore complex is nucleocytoplasmic transport of protein and RNA molecules[35]. However, a recent study suggests that loss of *Nup210* does not affect the general nucleocytoplasmic transport in differentiating myotubes[36]. To determine whether *Nup210* depletion affects nucleocytoplasmic transport in our metastatic 4T1 cancer cells, the NES-tdTomato-NLS nucleocytoplasmic transport reporter was used[36] (Supplementary Fig. 4a). This reporter expresses tdTomato protein fused to both a nuclear localization signal (NLS) and nuclear export signal (NES), resulting in shuttling between the cytoplasm and nucleus. Transfection of this reporter into *Nup210* knockdown 4T1 cells with or without the nuclear export inhibitor leptomycin B showed no significant differences in nucleocytoplasmic transport of the reporter protein

(Supplementary Fig. 4b). Next, we examined the effect of *Nup210* depletion on RNA export through oligo-d(T) RNA fluorescent *in situ* hybridization (FISH) analysis. Increased retention of polyA+ RNA signal was observed in the nucleus upon *Nup210* depletion (Supplementary Fig. 4c, 4d), implying that *Nup210* may facilitate RNA export into the cytoplasm.

NUP210 interacts with histone H3.1/3.2 at the nuclear periphery

To better understand how NUP210 promotes metastasis, co-immunoprecipitation (Co-IP) followed by mass spectrometry was performed to identify NUP210-interacting proteins (Fig. 4a). Interestingly, mass spectrometry analysis in NUP210-Myc overexpressing 4T1 cells revealed that both endogenous and Myc-tagged NUP210 potentially interact with multiple chromatin-associated molecules including histone H3.1 (Fig. 4b). Notably, mass spectrometry indicated that NUP210 also interacts with RRP1B, a chromatin-associated metastasis modifier gene previously identified by our lab[17,37]. Mutation of histone H3.1 has been reported in human cancer[38,39]. In the human breast cancer METABRIC dataset, amplification of histone H3.1 (*HIST1H3A* and *HIST1H3B*) might be associated with poor prognosis in breast cancer patients (P = 0.0642) (Fig. 4c). Despite this, the role of H3.1 in metastasis remains unclear. Since H3.1 can undergo post-translational modification to subsequently affect gene expression, we hypothesized that NUP210 interaction with histone H3.1 might regulate a gene expression program essential for metastatic progression. Reciprocal Co-IP in 4T1 cells using an antibody that recognizes both H3.1 and H3.2 validated the predicted H3.1-NUP210 interaction (Fig. 4d, 4e). H3.1/3.2 also pulled down lamin B1, a component of the nuclear lamina, suggesting that this interaction may occur at the nuclear periphery (Fig. 4e). Immunofluorescence analysis confirmed the association of H3.1/3.2 and

NUP210 at the nuclear periphery (Fig. 4f). These results establish the interaction of NUP210 with H3.1/3.2 and their localization in metastatic 4T1 cells.

Loss of NUP210 is associated with redistribution of H3.1/3.2 from the nuclear periphery to heterochromatin foci

We next investigated the role of NUP210-H3.1/3.2 interaction in our metastatic 4T1 cells. Since H3.1 is known to be incorporated into nucleosomes in S phase of the cell cycle in a replication-dependent manner[40], we initially speculated that NUP210 loss might affect S phase progression. However, DNA content analysis with EdU incorporation demonstrated that there was no consistent changes in cell cycle stage distribution (Supplementary Fig. 3a, 3b), suggesting that the function of NUP210-H3.1/3.2 association might be independent of cell cycle progression.

To investigate the cellular effect of *Nup210* loss on the distribution of H3.1 at the nuclear periphery, we performed super-resolution spinning disk microscopy in *Nup210* KO cells. Interestingly, H3.1/3.2 distribution at the nuclear periphery was significantly decreased (Fig. 4g, 4h) in *Nup210* KO cells, suggesting that H3.1/3.2 anchoring at the nuclear periphery might be reduced upon NUP210 loss. There was also significant enrichment of the H3K27me3 mark at the nuclear periphery in *Nup210* KO cells (Fig. 4g, 4h). H3.1/3.2 predominantly appeared as foci-like structures inside the nucleus upon knockout of *Nup210*. To determine if these H3.1/3.2 foci were associated with pericentric heterochromatin, we stained the cells for H3K9me3, a pericentric heterochromatin-associated histone modification marker. Upon *Nup210* KO, H3.1/3.2 accumulated on the periphery of H3K9me3-marked pericentric heterochromatin (Fig. 4i). We also observed a signficant increase in H3.1/3.2 staining at the heterochromatin foci marked by strong

DAPI signal (Fig. 4j). Although there was an overall increase in H3K9me3 within the nucleus, the distribution of H3K9me3 was not changed significantly following *Nup210* KO (Fig. 4j). Staining with a nucleolin antibody showed that many of the H3.1/3.2 foci appeared on the periphery of nucleoli, heterochromatin-enriched regions (Fig. 4k). As heterochromatin content can be inversely correlated with nuclear size[41], we measured the nuclear size and found it to be significantly decreased in *Nup210*-depleted and KO cells (Fig. 4l), indicative of increased chromatin compaction due to heterochromatinization. These results suggest that the loss of NUP210 is associated with redistribution of H3.1/3.2 to heterochromatin regions within the nucleus.

Increased recruitment of heterochromatin-modifying enzymes, SUV39H1 and EZH2, to H3.1/3.2 in Nup210 KO cells

Since we observed the redistribution of H3.1/3.2 to the heterochromatin regions upon *Nup210* KO, we wanted to investigate whether differential post-translational heterochromatin modification of H3.1/3.2 underlies the changes in distribution observed in *Nup210* KO cells. So, we performed H3.1/3.2 Co-IP with antibodies recognizing different heterochromatin modifications (H3K9me3 and H3K27me3) and the enzymes known to catalyze these modifications. Co-IP revealed that there was decreased association of H3.1/3.2 with lamin B1 and increased association with SUV39H1 (an enzyme catalyzing H3K9me3 modification of H3.1/3.2) as well as H3K9me3 in *Nup210* KO cells (Fig. 4m). Loss of NUP210 was also associated with increased interaction of H3.1/3.2 with EZH2 (Fig. 4n), a key component of the polycomb repressive complex 2 (PRC2) that catalyzes H3K27me3 deposition[42]. Further analysis of other PRC2 components revealed an increased association of EZH2 with SUZ12 (Fig. 4o) and H3K27me3 (Fig. 4p) upon *Nup210* KO. Taken together, these results suggests that NUP210 prevents the recruitment of heterochromatin-

modifying enzymes to H3.1/3.2. Loss of NUP210 may promote heterochromatin modification and thereby transcriptional suppression of H3.1/3.2-associated genes or regulatory elements (promoters, enhancers) required for metastatic progression.

NUP210 loss increases heterochromatin spreading on topologically associating domains and decreases expression of cell adhesion/migration-related genes

Since we observed increased heterochromatin association in *Nup210* KO cells, we hypothesized that NUP210 loss might lead to heterochromatinization of certain genomic region important for metastasis. Earlier studies have suggested that H3.1/3.2 is mainly associated with poised/bivalent gene promoters where it can undergo both activating (H3K4me3) and repressing (H3K27me3) modification[40]. Therefore, we performed chromatin immunoprecipitation analysis with massively parallel DNA sequencing (ChIP-seq) of NUP210, H3K27me3, and H3K4me3 to determine the pattern of genomic localization of these modifications in 4T1 cells. The majority (55.33%) of the NUP210 peaks were within intergenic regions (Fig. 5a). 19.01% of NUP210 peaks were found within 10 kb upstream of transcription start sites (TSS), while the rest of the peaks were found within gene bodies (i.e., exons, introns, and UTRs). Interestingly, enrichment profiling showed that NUP210 was mainly enriched in 3′-transcription end sites (TES) of the genes (Fig. 5b). Similar TES enrichment patterns have been observed for some transcriptional regulators[43] as well as nucleoporin, NUP153[44]. ChIP-seq of H3K27me3 in 4T1 cells revealed that there was a 40% (9962 peaks) overlap of the NUP210 peaks with H3K27me3 peaks (FDR < 0.05) (Fig. 5c). Overlaying the NUP210-enrichment profile with H3K27me3 in sg-Ctrl and *Nup210* KO cells revealed that H3K27me3 was enriched surrounding the NUP210-bound gene bodies (Fig. 5d). The ChIP-seq profile obtained using a pan-nuclear pore complex (NPC)-specific antibody (mAb414) did not

show a similar enrichment pattern, implying that this enrichment pattern is NUP210-specific. Interestingly, in *Nup210* KO cells, the H3K27me3 level was increased over NUP210-bound gene bodies (Fig. 5d), suggesting that these genes were undergoing H3K27me3-marked heterochromatinization. In addition, *Nup210* knockout led to overall spreading of H3K27me3 peak regions identified by the Sicer algorithm[45], suggesting that NUP210 loss might be associated with H3K27me3-marked heterochromatin spread (Fig. 5e). This result is consistent with our hypothesis that NUP210 might be protecting transcriptionally active chromatin regions from EZH2-mediated H3K27me3 heteterochromatin modification of H3.1/3.2 near the nuclear pore.

Since the majority (~60%) of NUP210 peaks (14945) did not overlap with H3K27me3 peaks (Fig. 5c), we speculated that NUP210 might also be protecting distal enhancers from H3K27me3-marked heterochromatin spreading. To investigate this, a publicly available H3K27 acetylation (H3K27Ac) active enhancer mark ChIP-seq dataset from mouse mammary luminal epithelial cells[27] was integrated into the analysis. NUP210 was found to be enriched at the edges of regions enriched for the H3K27Ac (Fig. 5f). Loss of NUP210 resulted in an increase in the repressive H3K27me3 mark across these enhancer regions, suggesting that NUP210 may be contributing to the prevention of heterochromatin spreading across distal regulator elements. Taken together, these data suggest that NUP210 may also play a role in preventing heterochromatic spread across enhancers and other distal transcriptional regulatory elements.

Earlier we observed that NUP210 knockout was associated with redistribution of H3.1/3.2 at heterochromatin regions. Our ChIP-seq data also suggest that NUP210 loss was associated with heterochromatin spreading over distal enhancers. Since enhancers are known to establish loops

with promoters to activate gene expression[46,47] and H3.1/3.2 is preferentially enriched at the poised promoters, we speculated that heterochromatin spread over enhancers due to NUP210 loss could also affect gene promoters. To assess this possibility, ChIP-seq of the transcriptional activation histone mark, H3K4me3, was performed in *Nup210* KO 4T1 cells. The TSS of 1199 genes showed 2-fold decreased enrichment of H3K4me3 upon *Nup210* knockout (Fig. 5g). As the loss of H3K4me3 at the promoter can be associated with decreased expression of genes, RNA-seq was performed in *Nup210* KD 4T1 cells, which identified 282 downregulated (2-fold) and 249 upregulated (2-fold) genes upon *Nup210* knockdown (Fig. 5h). Integration of the RNA-seq data revealed 62 genes that had loss of H3K4me3 at the promoter and ≥ 2-fold decreased expression (Fig. 5i). Gene Ontology (GO) analysis on those 62 genes showed enrichment of cell migration and chemotaxis processes (Fig. 5j), including chemokines (*Ccl2*, *Cxcl1*, *Cxcl3*), cytokine (*Il1a*), and cell adhesion (*Postn*, *Serpine1*, *Itga7*, *Itgb2*) molecules (Fig. 5k).

Since enhancer-promoter looping is thought to occur within distinct chromatin regions called topologically associated domains (TADs)[46], we hypothesized that NUP210 anchors TADs to the nuclear pore where distal promoter-enhancer loops are established. To determine whether these NUP210-regulated genes were associated with TADs, we analyzed publicly available Hi-C data from mouse embryonic stem cells (mESC)[48] using the 3D-Genome Browser[49] and integrated it with our own ChIP-seq data. Upon *Nup210* KO, H3K27me3 started accumulating across the *Cxcl* and *Ccl2* loci TADs (Fig. 5l), implying that NUP210 loss might disrupt the enhancer-promoter contacts for the *Cxcl*/*Ccl2* genes through heterochromatinization. Consisently, there was also a marked loss of H3K4me3 at the promoters of these genes. Examination of the *Cxcl* and *Ccl2* regions revealed that the enhancer-promoter interaction within the TADs may happen proximally

(~1.5 Mb for the *Cxcl* region) or distally (~17 Mb for the *Ccl2* region). These results suggest that NUP210 may prevent heterochromatinization of the certain TADs at the nuclear periphery.

Pharmacological inhibition of H3K27me3 heterochromatin modification restores the peripheral distribution of H3.1/3.2 and gene expression in Nup210 KO cells

To test our hypothesis that *Nup210* KO leads to H3K27me3-mediated heterochromatinization, we asked whether we could rescue the expression of the aforementioned cell migration-related genes (Fig. 5m) in *Nup210* KO cells through pharmacological inhibition of H3K27me3 modification with an EZH2 inhibitor (GSK126). Treatment with GSK126 significantly increased the expression of *Ccl2*, *Cxcl1*, *Cxcl3*, *Postn*, and *Il-1a* (Fig. 5n), suggesting that they were directly suppressed through heteterochromatinization in *Nup210* KO cells. On the other hand, GSK126 treatment decreased the expression of *Itga7*, *Itgb2*, and *Serpine1*, implying that they were either not directly suppressed by heteterochromatinization upon *Nup210* KO or could be suppressed by a non-specific effect of the drug. Next, we examined whether GSK126 altered the intra-nuclear distribution of H3.1/3.2. Interestingly, perinuclear distribution of H3.1/3.2 was significantly restored in GSK126-treated *Nup210* KO cells (Fig. 5o, 5p). This result suggests that the promoter/enhancers of these cell migration-relateds genes possesses H3.1/3.2 at the nuclear periphery and H3K27me3 modification of H3.1/3.2 is responsible for their suppressed expression in *Nup210* KO cells. Furthermore, the nuclear size was also significantly increased in GSK126-treated *Nup210* KO cells (Fig. 5q), suggesting that the reversal of heterochromatinization increases the nuclear size.

Nup210 loss is associated with differential repositioning of cell migration-related gene loci

To determine whether NUP210 regulates its target genes through anchoring certain TADs to the nuclear periphery, 3D-DNA FISH was performed to observe the localization of NUP210-regulated gene loci within the nucleus. FISH probes were generated from BAC clones (~2 Mb) overlapping the *Cxcl* region (*Cxcl3*, *Cxcl5*, *Cxcl15*, *Ppbp*, *Pf4*, *Gm36084*), *Postn* region (*Postn* and *Trpc4*), and *Ccl2* region (*Ccl2*, *Ccl7*, *Ccl11*, *Ccl12*, *Ccl8*, *Asic2*), and *Itgb2* region (*Itgb2*, *Fam207a*, *Pttg1ip*, *Sumo3*, *Ube2g2*). FISH analysis revealed that many of those gene loci were close to the nuclear periphery, suggesting that they were likely part of the TADs attached to the nuclear periphery (Fig. 6a). When we compared the relative positioning (nuclear periphery vs centroid) of FISH spots in sg-Ctrl and *Nup210* KO cells, *Cxcl*, *Postn*, and *Itgb2* gene loci were significantly repositioned upon *Nup210* KO (Fig. 6b). Radial positioning of *Ccl2*, however, was not significantly changed. Among the repositioned loci, *Cxcl* and *Itgb2* loci repositioned closer to the nuclear periphery, whereas *Postn* loci repositioned away from the periphery. Since some of the FISH spots were found near heterochromatin foci marked by dense DAPI signals, we asked whether these genes could be silenced through repositioning into heterochromatin foci. Interestingly, the distance of *Ccl2* FISH spots to heterochromatin foci were significantly reduced in *Nup210* KO (Fig. 6c) cells implying the silencing of the *Ccl2* loci may occur through repositioning into heterochromatin regions. These results suggest that NUP210 knockout is associated with altered chromatin topology and nuclear positioning of cell migration-related gene loci into chromatin regions where they are more likely to be repressed through heterochromatinization.

Nup210 is a mechanosensitive gene and regulates focal adhesion, cell migration, and invasion

The changes we observed in cell adhesion/migration-related gene expression upon NUP210 loss led us to hypothesize that NUP210 may affect metastatic progression by altering focal adhesion.

Staining for phospho-FAK (Y397) and phalloidin revealed that *Nup210* knockdown significantly decreased the number of focal adhesions in 4T1 and 6DT1 cells when plated on type I collagen matrix (Fig. 7a, 3b). *Nup210* knockdown also decreased the protein level of phospho-FAK without altering total FAK protein in 4T1 (Fig. 7c) and 6DT1 cells (Fig. 7d). Similar results were observed in *Nup210* KO 4T1 cells (Supplementary Fig. 5a, 5b). To further verify the effect of NUP210 loss on focal adhesion that we observed in mouse cells, knockdown of *NUP210* in two human breast cancer cell lines, MDA-MB-231 and MCF7, was performed. Similar to mouse cells, a decrease in p-FAK (Y397) without alteration of total FAK was observed in both of these cell lines (Supplementary Fig. 5c, 5d).

As focal adhesion is important for the cellular response to extracellular matrix (ECM) stiffness or mechanotransduction, we asked whether NUP210 is mechanosensitive in metastatic cells. 4T1 cells were plated on fibronectin-coated hydrogel matrices of different stiffness mimicking the ECM environment. In the soft/low stiffness (0.2 kPa) condition, 4T1 cells exhibited round colony-like morphology, while in the higher stiffness condition (12 kPa), these cells exhibited a more spread morphology (Fig. 7e). Western blot analysis revealed that the NUP210 protein level was increased in the higher stiffness condition (Fig. 7f), indicating that *Nup210* is mechanosensitive in 4T1 cells. The levels of p-FAK (Y397) and total FAK were also increased in this condition. Consistently, qRT-PCR analysis in soft and stiff matrices revealed that many NUP210-regulated genes were also mechanositive in 4T1 cells (Fig. 7g). In addition, *Nup210* knockdown cells exhibited decreased spreading in the higher stiffness condition (Fig. 7h), suggesting that NUP210 loss affects the mechanical response in metastatic 4T1 cells. As mechanotransduction can happen through alteration of cellular actin dynamics[50,51], we performed an actin polymerization assay in

Nup210 knockdown 4T1 cells. We treated 4T1 cells with an actin polymerization inhibitor, Cytochalasin D, and followed the recovery of actin polymerization over time. *Nup210* knockdown cells had decreased recovery of actin polymerization, as marked by phalloidin staining of actin stress fibers (Fig. 7i), suggesting that NUP210 can affect mechanostransduction through the alteration of actin dynamics.

As focal adhesion is critical for cell migration and invasion during the metastatic process, we investigated whether the depletion of NUP210 was associated with decreased migration and invasion of 4T1 and 6DT1 cells. Automated live-cell imaging analysis of cell migration showed that *Nup210* KO cells displayed significantly less random migration than sg-Ctrl 4T1 cells (Fig. 7j). A cell invasion assay using a matrigel-coated boyden chamber also revealed a significant reduction of cell invasion upon NUP210 depletion in 4T1 (Fig. 7k) and 6DT1 cells (Fig. 7l). Taken together, these results suggest that NUP210 is a cellular mechanosensor of the extracellular microenviroment, which is necessary for the metastatic behavior of cancer cells.

Nup210 regulates a pro-metastatic secretory phenotype that regulates focal adhesion, cell migration in vitro, and circulating tumor cells in mice

Since many of the NUP210-regulated genes were secretory molecules like cytokines (IL-1α), chemokines (CCL2, CXCL1, CXCL3), and adhesion molecules (POSTN, SERPINE1), we hypothesized that NUP210 might be regulating a secretory phenotype necessary for the metastatic potential of cancer cells. To test our hypothesis, we performed a cytokine array using the cultured supernatant of sh-Ctrl and *Nup210* knockdown cells. Consisent with the transcriptome data, decreased secretion of cytokines (IL-1α), chemokines (CCL2, CXCL1), and adhesion molecules

(POSTN, SERPINE1) was observed in *Nup210* knockdown 4T1 cells (Fig. 8a, 8b). To investigate whether NUP210 mediates its effect on focal adhesion and cell migration through altered secretory molecules, we chose to knockdown *Ccl2* as a candidate because it was the most dramatically decreased chemokine in *Nup210* knockdown cells and has known pro-metastatic roles[52-54]. Knockdown of *Ccl2* in 4T1 cells (Fig. 8c) dramatically reduced the p-FAK (Y397) levels without altering total FAK levels (Fig. 8d). A focal adhesion assay on a collagen type I matrix also showed that *Ccl2* knockdown cells had a round, less spread morphology and decreased focal adhesion foci (Fig. 8e). Automated live-cell analysis of cell migration revealed that there was a significant decrease in cell migration upon *Ccl2* knockdown phenocopying the loss of NUP210 in these cells (Fig. 8f). Amplification of *CCL2* has also been associated with poor prognosis in the METABRIC human breast cancer patient dataset (Fig. 8g).

During the metastatic process, disseminated tumor cells need to intravasate into the bloodstream and remain as circulating tumor cells (CTCs) until they adhere and extravasate into the surrounding organ to form a secondary tumor. CCL2 has been shown to have a direct role in tumor cell adhesion to the endothelial wall and facilitates extravasation during metastasis[55]. As *Nup210*-depleted cancer cells exhibited adhesion/migration defects and decreased secretion of CCL2, we hypothesized that NUP210 loss might affect the CTC population in mice. For these experiments, putative CTCs were isolated based on CD45-/CK+ staining[56]. A flow cytometry sample acquisition gate was created based on the staining pattern of 6DT1 cells in culture (Fig. 8h). Blood from healthy, tumor-free FVB/NJ mice was used as negative control. Under these conditions, approximately ~0.5-1% of the cells in the blood of 6DT1-sh-Ctrl tumor-bearing mice (at day 28) were CD45-/CK+ putative CTCs. In contrast, CTCs in mice with *Nup210*-depleted tumors were

indistinguishable from the FVB tumor-free control (Fig. 8h, 8i). These results suggest that NUP210 is either required for tumor cell extravasation from the primary tumor into the vasculature or for the survival of cells within the bloodstream.

Taken together, our model shows that NUP210 is a mechanical sensor of the extracellular microenviroment. In response to tissue stiffness, growth factors and integrins transmit the mechanical signal from the ECM to NUP210 to regulate the transcription of mechanosensitive genes (Fig. 8j), which in turn further activate downstream signaling pathways (e.g., actin polymerization, focal adhesion, etc.) necessary for cell migration and metastasis. In *Nup210* knockout cells, mechanical signals cannot pass through the cytoplasm to the nucleus to regulate mechanosensitive gene expression, thereby decreasing metastasis.

DISCUSSION:

The present study identified an interesting role for NUP210, a nuclear pore complex protein, in promoting cancer metastasis. To the best of our knowledge, we have uncovered a previously unknown mechanism for metastatic potential modulation through NUP210-dependent changes in chromatin accessibility over mechanosensitive, cell migration-related, pro-metastatic genes at the nuclear periphery.

Apart from providing structural support and general nucleocytoplasmic transport[35], the function of the nuclear pore complex in regulating gene expression has drawn much attention in recent years[57]. Although many of these studies are focused on developmental gene regulation[58-60], the function of nuclear pore complex components in human disease, especially cancer, has begun to emerge[19,20,61].

To date, NUP210 function has been implicated in muscle differentiation[36,62], cellular reprogramming[63], and T cell receptor signaling[64]. Here, we have identified *Nup210* as a potential metastasis susceptibility gene from the genome-wide screen of metastasis-associated polymorphism within gene promoters and enhancers. Germline polymorphism in the promoter region affect *Nup210* transcriptional activity through CTCF-dependent manner. Through patient dataset analysis, we found a significant association between high *NUP210* expression and poor outcome in human ER+ breast cancer patients. It would interesting to see whether the promoter polymorphism is responsible for the differential NUP210 expression among the breast cancer patients. Considering breast cancer as a heterogenous disease, further investigations will be required to elucidate the role of NUP210 in metastasis different subtypes of breast cancer.

Our study on the role of NUP210 has important implications in the field of cellular mechanosensing. Mechanical stress is important in the context of development[65] and cancer[66] because changes in extracellular matrix stiffness can affect embryogenesis, cell migration, angiogenesis, and metastasis. The nucleus is regarded as a sensor of mechanical stress upon exposure to different extracellular stimuli[67]. For instance, LINC (linker of nucleoskeleton and cytoskeleton), a nuclear envelope-anchored protein complex, serves as a mechanotransducer to regulate gene expression[68]. Furthermore, in response to mechanical stress, mechanosensitive transcription factors can translocate to the nucleus to regulate gene expression[50,51,69-71]. However, it remains unclear whether these gene expression changes occur due to alterations of 3D nuclear architecture or chromatin topology. Our results suggest that mechanosensitive, pro-metastatic genes can be activated by nuclear pore components through alteration of gene positioning and chromatin accessibility.

Strikingly, we observed that many of the NUP210-regulated mechanosensitive, cell migration-related genes were immune molecules like chemokines and cytokines. This specificity can be explained by the notion that the nuclear pore is thought of as a site of active transcription. Genes that need to be actively transcribed and transported to the cytoplasm for protein synthesis come into close proximity of the nuclear pore. Nuclear pore components also induce transcriptional memory for rapid activation of certain genes[72]. Transcriptional memory is essential for innate and adaptive immune responses where rapid transcriptional activation and secretion of immune molecules are required[73]. Interestingly, it was recently shown that upon stimulation, immune genes can be transcriptionally activated through alteration of topologically associating domains[74]. In response to a foreign ECM environment, metastatic cells may exploit this mechanism through repositioning TADs to the nuclear pore for robust transcription of mechanosensitive genes, which then promote their migration into distant organs in an autocrine fashion. In fact, two recent studies have suggested that *Nup210*-deficient mice possesses defective T-cell receptor signaling[64,75]. It is highly likely that NUP210 might promote metastasis through rapid transcriptional activation of mechanosensitive, immune component genes. Future studies will be needed to address the function of NUP210 in metastasis in the context of tumor cell-immune crosstalk.

Mechanistically, we have demonstrated that NUP210 interacts with histone H3.1/3.2 at the nuclear lamina. Histone H3.1/3.2 is considered as a DNA replication-coupled variant of histone H3. During DNA replication, H3.1/3.2 is usually deposited onto the newly synthesized DNA strand through its chaperones, CHAF1A and CHAF1B[76]. Recent reports have identified both pro-tumorigenic[77,78] and anti-metastatic[79] roles for CHAF1B in human malignancies, suggesting a cell

type-specific function of these H3.1/3.2 chaperones. Upon *Nup210* KO, we observed decreased enrichment of H3.1/3.2 at the nuclear periphery. Whether *Nup210* affects differential deposition of H3.1/3.2 by its chaperones and modulates pro-metastatic gene expression at the nuclear periphery requires further investigation.

In contrast to the peripheral localization of H3.1/3.2, we observed H3.1/3.2 enrichment at heterochromatin regions in *Nup210* KO cells. In support of this observation, we found increased association of heterochromatin-modifying enzymes (SUV39H1 and EZH2) with H3.1/3.2 and increased accumulation of H3K27me3-marked heterochromatin in *Nup210* KO cells. These results suggest a role for NUP210 as a chromatin barrier insulator-binding protein. The nuclear pore complex has been described as a chromatin barrier insulator component in yeast[80] and certain pore components have been shown to generate a zone of heterochromatin exclusion surrounding the nuclear pore[81]. Apart from some evidence in vertebrates, chromatin barrier insulators have not been well-characterized in mouse and human. Although the architectural protein CTCF is mainly considered to be an enhancer blocker[82], studies have suggested that it can also be associated with barrier insulators[83,84]. This barrier insulator contains actively transcribing euchromatin regions surrounded by heterochromatin marks. Loss of barrier insulator elements in the barrier region is associated with increased spreading of heterochromatin marks to adjacent actively transcribing gene loci, hence decreased global levels of histone acetylation and decreased enrichment of the activating H3K4me3 mark at gene promoters[85]. Since *Nup210* loss was associated with H3K27me3-marked heterochromatin spreading and loss of H3K4me3 from certain gene promoters, NUP210 might acts as a barrier of H3K27me3-mediated heterochromatinization to adjacent loci at the nuclear pore. We propose that NUP210 likely protects H3.1/3.2-associated

chromatin by preventing the recruitment of heterochromatin-modifying enzymes (SUV39H1 and EZH2) at the nuclear pore.

Our data suggest that NUP210 can also be enriched in the active enhancer regions and NUP210 loss was associated with increased enrichment of the H3K27me3 heterochromatin mark in those regions. Some of these chromatin regions repositioned differentially within the nucleus upon *Nup210* KO. This can be explained by the previous observation that nuclear pores can be a scaffold of enhancer-promoter contact mediating transcriptional activation of poised genes[60]. In addition, alteration of the nuclear lamina-chromatin interaction is reported to be essential for gene regulation during cellular differentiation[86]. So, it is conceivable that in response to higher stiffness of the extracellular microenvironment during metastatic progression, mechanical signals facilitate the interaction of NUP210 with histone H3.1/3.2-marked enhancer regions to establish distal regulatory element interaction with poised promoters of mechanosensitive genes. Hi-C data analysis also supports this possibility because NUP210-regulated genes reside within TADs, which are thought to possess H3K27Ac-marked regions surrounded by the insulator protein CTCF at the boundary[87]. The function of NUP210 in gene repositioning can also be linked to its ability to alter chromatin looping, as we showed *Nup210* to be a CTCF-regulated gene. It would be interesting to see whether this change in gene repositioning in *Nup210* KO cells is due to the repositioning of TAD boundaries from the active to silent chromatin compartments[88]. Further investigations are required to establish the role of CTCF-NUP210 axis in metastatic progression.

We showed that treating *Nup210* KO cells with an EZH2 inhibitor (GSK126) could partially rescue the peripheral distribution of H3.1/3.2 and mechanosensitive gene expression. This observation

has important clinical implications since EZH2 is a therapeutic target for multiple malignancies and some EZH2 inhibitors are currently in clinical trials[89,90]. In breast cancer, both tumor-promoting and inhibitory effects have been described for EZH2 in a context-specific manner[91]. Treating with an EZH2 inhibitor could adversely affect patient outcome through activation of mechanosensitive genes essential for cell migration and metastasis. In line with this speculation, GSK126 treatment has been shown to exhibit adverse effects via inhibiting anti-tumor immunity[92] and promoting inflammation[93] in pre-clinical models of cancer.

In conclusion, our current study has identified a previously unrecognized role for NUP210 in nuclear mechanosensing and promoting aggressive metastatic cancer that is independent of the general nucleocytoplasmic transport function of the nuclear pore. Since *Nup210* KO in breast cancer cell lines decreased metastasis through heterochromatinization of mechanosensitive genes, future studies should determine whether inhibiting NUP210-chromatin interactions can be a therapeutic strategy for aggressive metastatic disease.

ACKNOWLEDGEMENT:

The authors thank Sarah Deasy, Ngoc-Han Ha and Brandi Carofino for critical review of the manuscript. The authors also thank the Center for Cancer Research (CCR) Flow Cytometry Core Facility members, including Ferenc Livak, Karen Wolcott, and Caiyi Cherry Li, for FACS analysis. RNA-seq and ChIP-seq analysis was performed by the CCR sequencing facility at the National Cancer Institute, Frederick, MD. LC-MS analysis was performed by the CCR mass spectrometry core facility at NCI Frederick. This research was supported by the Intramural Research Program of the National Institutes of Health, National Cancer Institute, Center for Cancer

Research. The funder has no role in study design, data collection and analysis, decision to publish or preparation of the manuscript.

AUTHOR CONTRIBUTIONS:

R.A conceived the project, performed the majority of the experiments, analyzed the data, and wrote the manuscript. A.S, J.J.Z, S.K, P.W, and S.Z.T performed chromatin accessibility, ChIA-PET analysis, and wrote the manuscript. S.B performed DNA FISH analysis. H.L and M.P.L performed ChIP-seq/RNA-seq analysis. S.D.C analyzed the automated live-cell imaging of cell migration. A.T and M.J.K performed microscopy image analysis and wrote the manuscript. G.L.H provided expertise and supervised the chromatin accessibility analysis. Y.R provided expertise and supervised the ChIA-PET analysis. K.W.H conceived and supervised the whole project, analyzed the data, and wrote the manuscript.

DECLARATION OF INTERESTS:

Authors have declared that there is no conflict of interests.

REFERENCES:

1. Hunter, K.W., Amin, R., Deasy, S., Ha, N.H. & Wakefield, L. Genetic insights into the morass of metastatic heterogeneity. *Nat Rev Cancer* **18**, 211-223 (2018).
2. Nguyen, D.X., Bos, P.D. & Massague, J. Metastasis: from dissemination to organ-specific colonization. *Nat Rev Cancer* **9**, 274-84 (2009).

3. Sethi, N. & Kang, Y. Unravelling the complexity of metastasis - molecular understanding and targeted therapies. *Nat Rev Cancer* **11**, 735-48 (2011).

4. Steeg, P.S. Targeting metastasis. *Nat Rev Cancer* **16**, 201-18 (2016).

5. Garraway, L.A. & Lander, E.S. Lessons from the cancer genome. *Cell* **153**, 17-37 (2013).

6. Robinson, D.R. *et al.* Integrative clinical genomics of metastatic cancer. *Nature* **548**, 297-303 (2017).

7. Campbell, P.J. *et al.* The patterns and dynamics of genomic instability in metastatic pancreatic cancer. *Nature* **467**, 1109-13 (2010).

8. Yates, L.R. *et al.* Genomic Evolution of Breast Cancer Metastasis and Relapse. *Cancer Cell* **32**, 169-184 e7 (2017).

9. Makohon-Moore, A.P. *et al.* Limited heterogeneity of known driver gene mutations among the metastases of individual patients with pancreatic cancer. *Nat Genet* **49**, 358-366 (2017).

10. Berdasco, M. & Esteller, M. Aberrant epigenetic landscape in cancer: how cellular identity goes awry. *Dev Cell* **19**, 698-711 (2010).

11. Chatterjee, A., Rodger, E.J. & Eccles, M.R. Epigenetic drivers of tumourigenesis and cancer metastasis. *Semin Cancer Biol* **51**, 149-159 (2018).

12. Kazanets, A., Shorstova, T., Hilmi, K., Marques, M. & Witcher, M. Epigenetic silencing of tumor suppressor genes: Paradigms, puzzles, and potential. *Biochim Biophys Acta* **1865**, 275-88 (2016).

13. Denny, S.K. *et al.* Nfib Promotes Metastasis through a Widespread Increase in Chromatin Accessibility. *Cell* **166**, 328-342 (2016).

14. McDonald, O.G. *et al.* Epigenomic reprogramming during pancreatic cancer progression links anabolic glucose metabolism to distant metastasis. *Nat Genet* **49**, 367-376 (2017).

15. Alsarraj, J. *et al.* BRD4 short isoform interacts with RRP1B, SIPA1 and components of the LINC complex at the inner face of the nuclear membrane. *PLoS One* **8**, e80746 (2013).

16. Park, Y.G. *et al.* Sipa1 is a candidate for underlying the metastasis efficiency modifier locus Mtes1. *Nat Genet* **37**, 1055-62 (2005).

17. Crawford, N.P., Yang, H., Mattaini, K.R. & Hunter, K.W. The metastasis efficiency modifier ribosomal RNA processing 1 homolog B (RRP1B) is a chromatin-associated factor. *J Biol Chem* **284**, 28660-73 (2009).

18. Sakuma, S. & D'Angelo, M.A. The roles of the nuclear pore complex in cellular dysfunction, aging and disease. *Semin Cell Dev Biol* **68**, 72-84 (2017).

19. Kohler, A. & Hurt, E. Gene regulation by nucleoporins and links to cancer. *Mol Cell* **38**, 6-15 (2010).

20. Xu, H. *et al.* NUP98 Fusion Proteins Interact with the NSL and MLL1 Complexes to Drive Leukemogenesis. *Cancer Cell* **30**, 863-878 (2016).

21. Rodriguez-Bravo, V. *et al.* Nuclear Pores Promote Lethal Prostate Cancer by Increasing POM121-Driven E2F1, MYC, and AR Nuclear Import. *Cell* **174**, 1200-1215 e20 (2018).

22. Aslakson, C.J. & Miller, F.R. Selective events in the metastatic process defined by analysis of the sequential dissemination of subpopulations of a mouse mammary tumor. *Cancer Res* **52**, 1399-405 (1992).

23. Nishizaki, S.S. & Boyle, A.P. Mining the Unknown: Assigning Function to Noncoding Single Nucleotide Polymorphisms. *Trends Genet* **33**, 34-45 (2017).

24. Churchill, G.A., Gatti, D.M., Munger, S.C. & Svenson, K.L. The Diversity Outbred mouse population. *Mamm Genome* **23**, 713-8 (2012).

25. Keane, T.M. *et al.* Mouse genomic variation and its effect on phenotypes and gene regulation. *Nature* **477**, 289-94 (2011).

26. Willi, M. *et al.* Facultative CTCF sites moderate mammary super-enhancer activity and regulate juxtaposed gene in non-mammary cells. *Nat Commun* **8**, 16069 (2017).

27. Dravis, C. *et al.* Epigenetic and Transcriptomic Profiling of Mammary Gland Development and Tumor Models Disclose Regulators of Cell State Plasticity. *Cancer Cell* **34**, 466-482 e6 (2018).

28. Ghirlando, R. & Felsenfeld, G. CTCF: making the right connections. *Genes Dev* **30**, 881-91 (2016).

29. Tang, Z. *et al.* CTCF-Mediated Human 3D Genome Architecture Reveals Chromatin Topology for Transcription. *Cell* **163**, 1611-27 (2015).

30. Phillips, J.E. & Corces, V.G. CTCF: master weaver of the genome. *Cell* **137**, 1194-211 (2009).

31. Curtis, C. *et al.* The genomic and transcriptomic architecture of 2,000 breast tumours reveals novel subgroups. *Nature* **486**, 346-52 (2012).

32. Gyorffy, B. *et al.* An online survival analysis tool to rapidly assess the effect of 22,277 genes on breast cancer prognosis using microarray data of 1,809 patients. *Breast Cancer Res Treat* **123**, 725-31 (2010).

33. Pei, X.F. *et al.* Explant-cell culture of primary mammary tumors from MMTV-c-Myc transgenic mice. *In Vitro Cell Dev Biol Anim* **40**, 14-21 (2004).

34. Yang, Y. *et al.* Immunocompetent mouse allograft models for development of therapies to target breast cancer metastasis. *Oncotarget* **8**, 30621-30643 (2017).

35. Beck, M. & Hurt, E. The nuclear pore complex: understanding its function through structural insight. *Nat Rev Mol Cell Biol* **18**, 73-89 (2017).

36. D'Angelo, M.A., Gomez-Cavazos, J.S., Mei, A., Lackner, D.H. & Hetzer, M.W. A change in nuclear pore complex composition regulates cell differentiation. *Dev Cell* **22**, 446-58 (2012).

37. Crawford, N.P. *et al.* Rrp1b, a new candidate susceptibility gene for breast cancer progression and metastasis. *PLoS Genet* **3**, e214 (2007).

38. Mackay, A. *et al.* Integrated Molecular Meta-Analysis of 1,000 Pediatric High-Grade and Diffuse Intrinsic Pontine Glioma. *Cancer Cell* **32**, 520-537 e5 (2017).

39. Taylor, K.R. *et al.* Recurrent activating ACVR1 mutations in diffuse intrinsic pontine glioma. *Nat Genet* **46**, 457-461 (2014).

40. Loyola, A. & Almouzni, G. Marking histone H3 variants: how, when and why? *Trends Biochem Sci* **32**, 425-33 (2007).

41. Linhoff, M.W., Garg, S.K. & Mandel, G. A high-resolution imaging approach to investigate chromatin architecture in complex tissues. *Cell* **163**, 246-55 (2015).

42. Margueron, R. & Reinberg, D. The Polycomb complex PRC2 and its mark in life. *Nature* **469**, 343-9 (2011).

43. Wen, H. *et al.* ZMYND11 links histone H3.3K36me3 to transcription elongation and tumour suppression. *Nature* **508**, 263-8 (2014).

44. Toda, T. *et al.* Nup153 Interacts with Sox2 to Enable Bimodal Gene Regulation and Maintenance of Neural Progenitor Cells. *Cell Stem Cell* **21**, 618-634 e7 (2017).

45. Xu, S., Grullon, S., Ge, K. & Peng, W. Spatial clustering for identification of ChIP-enriched regions (SICER) to map regions of histone methylation patterns in embryonic stem cells. *Methods Mol Biol* **1150**, 97-111 (2014).

46. Dixon, J.R., Gorkin, D.U. & Ren, B. Chromatin Domains: The Unit of Chromosome Organization. *Mol Cell* **62**, 668-80 (2016).

47. Hnisz, D., Day, D.S. & Young, R.A. Insulated Neighborhoods: Structural and Functional Units of Mammalian Gene Control. *Cell* **167**, 1188-1200 (2016).

48. Bonev, B. *et al.* Multiscale 3D Genome Rewiring during Mouse Neural Development. *Cell* **171**, 557-572 e24 (2017).

49. Wang, Y. *et al.* The 3D Genome Browser: a web-based browser for visualizing 3D genome organization and long-range chromatin interactions. *Genome Biol* **19**, 151 (2018).

50. Ho, C.Y., Jaalouk, D.E., Vartiainen, M.K. & Lammerding, J. Lamin A/C and emerin regulate MKL1-SRF activity by modulating actin dynamics. *Nature* **497**, 507-11 (2013).

51. Jaalouk, D.E. & Lammerding, J. Mechanotransduction gone awry. *Nat Rev Mol Cell Biol* **10**, 63-73 (2009).

52. Qian, B.Z. *et al.* CCL2 recruits inflammatory monocytes to facilitate breast-tumour metastasis. *Nature* **475**, 222-5 (2011).

53. Wolf, M.J. *et al.* Endothelial CCR2 signaling induced by colon carcinoma cells enables extravasation via the JAK2-Stat5 and p38MAPK pathway. *Cancer Cell* **22**, 91-105 (2012).

54. Bonapace, L. *et al.* Cessation of CCL2 inhibition accelerates breast cancer metastasis by promoting angiogenesis. *Nature* **515**, 130-3 (2014).

55. Reymond, N., d'Agua, B.B. & Ridley, A.J. Crossing the endothelial barrier during metastasis. *Nat Rev Cancer* **13**, 858-70 (2013).

56. Alvarez Cubero, M.J. *et al.* Circulating Tumor Cells: Markers and Methodologies for Enrichment and Detection. *Methods Mol Biol* **1634**, 283-303 (2017).

57. Raices, M. & D'Angelo, M.A. Nuclear pore complexes and regulation of gene expression. *Curr Opin Cell Biol* **46**, 26-32 (2017).

58. Kalverda, B., Pickersgill, H., Shloma, V.V. & Fornerod, M. Nucleoporins directly stimulate expression of developmental and cell-cycle genes inside the nucleoplasm. *Cell* **140**, 360-71 (2010).

59. Capelson, M. *et al.* Chromatin-bound nuclear pore components regulate gene expression in higher eukaryotes. *Cell* **140**, 372-83 (2010).

60. Pascual-Garcia, P. *et al.* Metazoan Nuclear Pores Provide a Scaffold for Poised Genes and Mediate Induced Enhancer-Promoter Contacts. *Mol Cell* **66**, 63-76 e6 (2017).

61. Wang, G.G., Cai, L., Pasillas, M.P. & Kamps, M.P. NUP98-NSD1 links H3K36 methylation to Hox-A gene activation and leukaemogenesis. *Nat Cell Biol* **9**, 804-12 (2007).

62. Raices, M. *et al.* Nuclear Pores Regulate Muscle Development and Maintenance by Assembling a Localized Mef2C Complex. *Dev Cell* **41**, 540-554 e7 (2017).

63. Hansson, J. *et al.* Highly coordinated proteome dynamics during reprogramming of somatic cells to pluripotency. *Cell Rep* **2**, 1579-92 (2012).

64. Borlido, J. *et al.* Nuclear pore complex-mediated modulation of TCR signaling is required for naive CD4(+) T cell homeostasis. *Nat Immunol* **19**, 594-605 (2018).

65. Wozniak, M.A. & Chen, C.S. Mechanotransduction in development: a growing role for contractility. *Nat Rev Mol Cell Biol* **10**, 34-43 (2009).

66. Chin, L., Xia, Y., Discher, D.E. & Janmey, P.A. Mechanotransduction in cancer. *Curr Opin Chem Eng* **11**, 77-84 (2016).

67. Kirby, T.J. & Lammerding, J. Emerging views of the nucleus as a cellular mechanosensor. *Nat Cell Biol* **20**, 373-381 (2018).

68. Wang, N., Tytell, J.D. & Ingber, D.E. Mechanotransduction at a distance: mechanically coupling the extracellular matrix with the nucleus. *Nat Rev Mol Cell Biol* **10**, 75-82 (2009).

69. Janmey, P.A., Wells, R.G., Assoian, R.K. & McCulloch, C.A. From tissue mechanics to transcription factors. *Differentiation* **86**, 112-20 (2013).

70. Dupont, S. *et al.* Role of YAP/TAZ in mechanotransduction. *Nature* **474**, 179-83 (2011).

71. Elosegui-Artola, A. *et al.* Force Triggers YAP Nuclear Entry by Regulating Transport across Nuclear Pores. *Cell* **171**, 1397-1410 e14 (2017).

72. Light, W.H. & Brickner, J.H. Nuclear pore proteins regulate chromatin structure and transcriptional memory by a conserved mechanism. *Nucleus* **4**, 357-60 (2013).

73. Woodworth, A.M. & Holloway, A.F. The Role of Epigenetic Regulation in Transcriptional Memory in the Immune System. *Adv Protein Chem Struct Biol* **106**, 43-69 (2017).

74. Fanucchi, S. *et al.* Immune genes are primed for robust transcription by proximal long noncoding RNAs located in nuclear compartments. *Nat Genet* **51**, 138-150 (2019).

75. van Nieuwenhuijze, A. *et al.* Mice Deficient in Nucleoporin Nup210 Develop Peripheral T Cell Alterations. *Front Immunol* **9**, 2234 (2018).

76. Tagami, H., Ray-Gallet, D., Almouzni, G. & Nakatani, Y. Histone H3.1 and H3.3 complexes mediate nucleosome assembly pathways dependent or independent of DNA synthesis. *Cell* **116**, 51-61 (2004).

77. Volk, A. *et al.* A CHAF1B-Dependent Molecular Switch in Hematopoiesis and Leukemia Pathogenesis. *Cancer Cell* **34**, 707-723 e7 (2018).

78. Peng, X., Fu, H., Yin, J. & Zhao, Q. CHAF1B knockdown blocks migration in a hepatocellular carcinoma model. *Oncol Rep* **40**, 405-413 (2018).

79. Gomes, A.P. *et al.* Dynamic Incorporation of Histone H3 Variants into Chromatin Is Essential for Acquisition of Aggressive Traits and Metastatic Colonization. *Cancer Cell* **36**, 402-417 e13 (2019).

80. Ishii, K., Arib, G., Lin, C., Van Houwe, G. & Laemmli, U.K. Chromatin boundaries in budding yeast: the nuclear pore connection. *Cell* **109**, 551-62 (2002).

81. Krull, S. *et al.* Protein Tpr is required for establishing nuclear pore-associated zones of heterochromatin exclusion. *EMBO J* **29**, 1659-73 (2010).

82. Gaszner, M. & Felsenfeld, G. Insulators: exploiting transcriptional and epigenetic mechanisms. *Nat Rev Genet* **7**, 703-13 (2006).

83. Cuddapah, S. *et al.* Global analysis of the insulator binding protein CTCF in chromatin barrier regions reveals demarcation of active and repressive domains. *Genome Res* **19**, 24-32 (2009).

84. Narendra, V. *et al.* CTCF establishes discrete functional chromatin domains at the Hox clusters during differentiation. *Science* **347**, 1017-21 (2015).

85. West, A.G., Huang, S., Gaszner, M., Litt, M.D. & Felsenfeld, G. Recruitment of histone modifications by USF proteins at a vertebrate barrier element. *Mol Cell* **16**, 453-63 (2004).

86. Poleshko, A. *et al.* Genome-Nuclear Lamina Interactions Regulate Cardiac Stem Cell Lineage Restriction. *Cell* **171**, 573-587 e14 (2017).

87. Spielmann, M., Lupianez, D.G. & Mundlos, S. Structural variation in the 3D genome. *Nat Rev Genet* **19**, 453-467 (2018).

88. Gonzalez-Sandoval, A. & Gasser, S.M. On TADs and LADs: Spatial Control Over Gene Expression. *Trends Genet* **32**, 485-495 (2016).

89. Stazi, G., Zwergel, C., Mai, A. & Valente, S. EZH2 inhibitors: a patent review (2014-2016). *Expert Opin Ther Pat* **27**, 797-813 (2017).

90. Tremblay-LeMay, R., Rastgoo, N., Pourabdollah, M. & Chang, H. EZH2 as a therapeutic target for multiple myeloma and other haematological malignancies. *Biomark Res* **6**, 34 (2018).

91. Lee, S.T. *et al.* Context-specific regulation of NF-kappaB target gene expression by EZH2 in breast cancers. *Mol Cell* **43**, 798-810 (2011).

92. Huang, S. *et al.* EZH2 Inhibitor GSK126 Suppresses Antitumor Immunity by Driving Production of Myeloid-Derived Suppressor Cells. *Cancer Res* **79**, 2009-2020 (2019).

93. Serresi, M. *et al.* Ezh2 inhibition in Kras-driven lung cancer amplifies inflammation and associated vulnerabilities. *J Exp Med* **215**, 3115-3135 (2018).

94. Grontved, L. *et al.* Rapid genome-scale mapping of chromatin accessibility in tissue. *Epigenetics Chromatin* **5**, 10 (2012).

95. John, S. *et al.* Chromatin accessibility pre-determines glucocorticoid receptor binding patterns. *Nat Genet* **43**, 264-8 (2011).

96. Baek, S., Sung, M.H. & Hager, G.L. Quantitative analysis of genome-wide chromatin remodeling. *Methods Mol Biol* **833**, 433-41 (2012).

97. Fujiwara, S., Baek, S., Varticovski, L., Kim, S. & Hager, G.L. High Quality ATAC-Seq Data Recovered from Cryopreserved Breast Cell Lines and Tissue. *Sci Rep* **9**, 516 (2019).

98. Li, X. *et al.* Long-read ChIA-PET for base-pair-resolution mapping of haplotype-specific chromatin interactions. *Nat Protoc* **12**, 899-915 (2017).

99. Ramirez, F. *et al.* deepTools2: a next generation web server for deep-sequencing data analysis. *Nucleic Acids Res* **44**, W160-5 (2016).

100. Yu, G., Wang, L.G. & He, Q.Y. ChIPseeker: an R/Bioconductor package for ChIP peak annotation, comparison and visualization. *Bioinformatics* **31**, 2382-3 (2015).

101. Robinson, J.T. *et al.* Integrative genomics viewer. *Nat Biotechnol* **29**, 24-6 (2011).

102. Mi, H. *et al.* Protocol Update for large-scale genome and gene function analysis with the PANTHER classification system (v.14.0). *Nat Protoc* **14**, 703-721 (2019).

103. Cappell, S.D., Chung, M., Jaimovich, A., Spencer, S.L. & Meyer, T. Irreversible APC(Cdh1) Inactivation Underlies the Point of No Return for Cell-Cycle Entry. *Cell* **166**, 167-80 (2016).

104. Ringner, M., Fredlund, E., Hakkinen, J., Borg, A. & Staaf, J. GOBO: gene expression-based outcome for breast cancer online. *PLoS One* **6**, e17911 (2011).

105. Cerami, E. *et al.* The cBio cancer genomics portal: an open platform for exploring multidimensional cancer genomics data. *Cancer Discov* **2**, 401-4 (2012).

106. Schindelin, J. *et al.* Fiji: an open-source platform for biological-image analysis. *Nat Methods* **9**, 676-82 (2012).

107. Ollion, J., Cochennec, J., Loll, F., Escude, C. & Boudier, T. TANGO: a generic tool for high-throughput 3D image analysis for studying nuclear organization. *Bioinformatics* **29**, 1840-1 (2013).

FIGURE LEGENDS:

Figure 1: Genome-wide analysis of non-coding region polymorphisms identifies *Nup210* as a metastasis susceptibility gene in breast cancer.

(a) Identification scheme for metastasis susceptibility genes associated with polymorphic Benzonase-accessible chromatin (BACH) regions.

(b) Circos plot representation of the 52 genes (marked by blue color on the outer area of the plot) and their chromosomal locations that showed metastasis association in the mouse diversity outbred panel. Some of these genes have polymorphic promoters (red lines). Some of them showed intra- (blue lines) and inter-chromosomal (light blue lines) looping interactions.

(c) Distant metastasis-free survival of human ER+ breast cancer patients stratified by their expression of the 52-gene signature derived from the genes shown in (b). Patient data were obtained from the METABRIC dataset.

(d) RNA-seq analysis of *Nup210* mRNA expression in the 4T1 series of breast cancer cells. Dots represent two biological replicates.

(e) Integrative genomic viewer (IGV) track showing the mouse *Nup210* promoter BACH region in 4T07 and 4T1 cell line. A 510 bp region (purple box) was analyzed for promoter polymorphisms.

(f) Individual polymorphisms (SNPs, indels) identified within the 510 bp *Nup210* promoter region from different mouse strains.

(g) 12 bp insertion in the *Nup210* promoter of the FVB/NJ strain is located within the active enhancer (H3K27Ac-marked)-promoter (H3K4me3) region. This particular region also

showed the enrichment of CTCF. ME, mammary epithelial cells; ML, mammary luminal cells.

(h) Differential enrichment of CTCF and H3K27Ac at the *Nup210* promoter region between mouse metastatic 4T1 (BALB/cJ tumor-derived) and 6DT1 (FVB/NJ tumor-derived) cell lines.

(i) Comparison of *Nup210* and *Ctcf* mRNA levels between 4T1 and 6DT1 cell lines. ***P < 0.001.

(j) Comparison of *Nup210* and *Ctcf* mRNA levels in the spleen of normal BALB/cJ and FVB/NJ mouse strains. *P < 0.05, NS = non-significant.

(k) Relative luciferase activity of the *Nup210* promoter regions derived from the BALB/cJ and FVB/NJ strains. ****P < 0.0001.

(l) *Ctcf* knockdown effect on the *Nup210* mRNA level in 4T1 cells. *P < 0.05, **P < 0.01, ***P < 0.001.

(m) *Ctcf* knockdown effect on the NUP210 protein level in 4T1 cells.

Figure 2: *NUP210* expression is associated with poor survival outcome in human ER+ breast cancer patients.

(a) Effect of *NUP210* amplification on the overall survival of breast cancer patients from the METABRIC dataset.

(b) Effect of *NUP210* mRNA expression level on the overall survival of ER+ breast cancer patients from the METABRIC dataset.

(c) Effect of *NUP210* mRNA expression level on the overall survival of ER-/PR-/Her2- breast cancer patients from the METABRIC dataset.

(d) Effect of *NUP210* mRNA expression level on distant metastasis-free survival of ER+ breast cancer patients (Km-plotter).

(e) Effect of *NUP210* mRNA expression level on distant metastasis-free survival of ER-/PR-/Her2- breast cancer patients (Km-plotter).

(f) *NUP210* mRNA expression level within different PAM50 breast cancer molecular subtypes from the METABRIC dataset. Kruskal-Wallis test. ****P < 0.0001, NS = non-significant.

(g) Human breast cancer dataset showing the *NUP210* mRNA expression level in multiple metastatic sites. Kruskal-Wallis test. *P < 0.05, **P < 0.01.

(h) Human prostate cancer dataset showing the differential expression of *NUP210* mRNA between primary tumor and metastases. Mann-Whitney U test. ****P < 0.0001.

(i) Human melanoma dataset showing the differential expression of *NUP210* mRNA between primary tumor and metastases. Mann-Whitney U test. *P < 0.05.

Figure 3: Depletion of *Nup210* in 4T1 metastatic cancer cells reduces lung metastasis in mice.

(a) Western blot showing shRNA-mediated stable *Nup210* knockdown (KD) in the 4T1 metastatic mouse mammary cancer cell line.

(b) Primary tumor weight after orthotopic transplantation of *Nup210* knockdown 4T1 cells. ***P < 0.001, NS = non-significant.

(c) Lung metastases count after orthotopic transplantation of *Nup210* knockdown 4T1 cells. *P < 0.05, **P < 0.01.

(d) Lung metastases count normalized to primary tumor weight, derived from values shown in (b) and (c). *P < 0.05, **P < 0.01.

(e) Western blot showing the CRISPR/Cas9-mediated knockout (KO) of *Nup210* in 4T1 cells. Two clones, N9 and N13, are shown. The sg-Ctrl 4T1 cells were established using a non-targeting sgRNA.

(f) Primary tumor weight, (g) lung metastases count, and (h) tumor-normalized metastases count after orthotopic transplantation of *Nup210* KO 4T1 cells. **P < 0.01, ***P < 0.001, **** < 0.0001.

(i) Western blot (left) and qRT-PCR (right) showing the overexpression (OE) of NUP210 in 4T1 cells. *P < 0.05.

(j) Primary tumor weight and (k) lung metastases count after orthotopic transplantation of NUP210-overexpressing 4T1 cells. **P < 0.01, NS = non-significant.

Figure 4: NUP210 interacts with histone H3.1/3.2 at the nuclear periphery and the loss of NUP210 is associated with re-distribution of H3.1/3.2 from the nuclear periphery to heterochromatin foci.

(a) Schematic of NUP210 co-immunoprecipitation (Co-IP) followed by LC-MS analysis.

(b) Number of peptides identified from two biological replicates in LC-MS analysis using both endogenous NUP210-specific and Myc-tag (NUP210-Myc)-specific antibodies.

(c) Effect of histone H3.1 amplification on the overall survival of human breast cancer patients (METABRIC dataset).

(d) Validation of NUP210-Myc interaction with H3.1/3.2 with Co-IP using lysates from 4T1 cells with NUP210-Myc OE.

(e) Co-IP showing the endogenous H3.1/3.2 interaction with endogenous NUP210 and lamin B1 in 4T1 cells.

(f) Representative images from immunofluorescence analysis showing the localization of H3.1/3.2 (green) with NUP210-Myc (red) at the nuclear periphery in 4T1 cells. DNA is labeled with DAPI (blue). Scale bar = 5 μm.

(g) Representative super-resolution spinning disk microscope images showing the distribution of H3.1/3.2 (green) and H3K27me3 (red) in sg-Ctrl and *Nup210* KO (KO-N13) 4T1 cells. DNA is labeled with DAPI (blue). Scale bar = 5 μm.

(h) Quantification of the ratio of H3.1/3.2 and H3K27me3 intensity distribution at the nuclear periphery vs total intensity within the nucleus in sg-Ctrl and *Nup210* KO (KO-N13) 4T1 cells. For H3.1/3.2, ****$P < 0.0001$, n = 87 for sg-Ctrl and n = 130 for KO-N13. For H3K27me3, *$P < 0.05$, n = 61 for sg-Ctrl and n = 63 for KO-N13.

(i) Representative super-resolution spinning disk microscope images showing H3.1/3.2 (green) localized on the periphery of pericentric heterochromatin (H3K9me3; red) in sg-Ctrl and *Nup210* KO (KO-N13) 4T1 cells. DNA is labeled with DAPI (blue). Scale bar = 5 μm.

(j) Quantification of the ratio of H3.1/3.2 intensity distribution at heterochromatin foci vs total H3.1/3.2 intensity within the nucleus in sg-Ctrl and *Nup210* KO (KO-N13) 4T1 cells. ****$P < 0.0001$, n = 1182 foci for sg-Ctrl and n = 1513 foci for KO-N13. Quantification of the ratio of H3K9me3 intensity at the nuclear periphery vs total H3K9me3 intensity within the nucleus in sg-Ctrl and *Nup210* KO (KO-N13) 4T1 cells. NS = non-significant, n = 79 for sg-Ctrl and n = 97 for KO-N13.

(k) Confocal immunofluorescence analysis showing H3.1/3.2 (green) distribution in sg-Ctrl and *Nup210* KO (KO-N13) 4T1 cells at the periphery of the nucleolus (nucleolin; red). DNA is labeled with DAPI (blue). Scale bar = 5 μm.

(l) Quantification of the nuclear area in *Nup210* KO (sg-Ctrl, n = 70; KO-N9, n = 164; KO-N13, n = 119) and KD (sh-Ctrl, n = 277; sh-Nup # 1, n = 229; sh-Nup # 4, n = 327) 4T1 cells. ****P < 0.0001.

(m) Co-IP showing the interaction of H3.1/3.2 with lamin B1, SUV39H1, and H3K9me3 in sg-Ctrl and *Nup210* KO (KO-N13) 4T1 cells.

(n) Co-IP showing the interaction of H3.1/3.2 with the PRC2 complex component, EZH2, in sg-Ctrl and *Nup210* KO (KO-N13) 4T1 cells.

(o) Co-IP showing the interaction between PRC2 complex components, EZH2 and SUZ12, in sg-Ctrl and *Nup210* KO (KO-N13) 4T1 cells.

(p) Co-IP showing the interaction of EZH2 with H3K27me3 in sg-Ctrl and *Nup210* KO (KO-N13) 4T1 cells.

Figure 5: Loss of NUP210 is associated with H3K27me3-marked heterochromatin spreading on topologically associating domains (TADs).

(a) NUP210 ChIP-seq peak distribution in different genomic regions in 4T1 cells.

(b) Normalized profile of NUP210 ChIP-seq peak enrichment over gene bodies in 4T1 cells.

(c) Overlap of NUP210 and H3K27me3 ChIP-seq peaks in 4T1 cells. TSS = Transcriptional start site, TES = Transcriptional end site.

(d) H3K27me3 ChIP-seq peak enrichment over gene bodies in sg-Ctrl (red) and *Nup210* KO (KO-N13) (blue) 4T1 cells within NUP210-enriched regions (purple). The ChIP-seq profile derived using an anti-Nuclear Pore Complex (NPC)-specific antibody was plotted as negative control (green).

(e) Normalized ChIP-seq profile showing the expansion of H3K27me3 peaks identified by the Sicer algorithm in sg-Ctrl (red) and *Nup210* KO (KO-N13) (blue) 4T1 cells.

(f) Normalized ChIP-seq profile showing the occupancy of H3K27me3 peaks within the NUP210-H3K27Ac (purple, green) enhancer overlap region in sg-Ctrl (red) and *Nup210* KO (KO-N13) (blue) 4T1 cells.

(g) Normalized ChIP-seq profile of H3K4me3 enrichment over gene promoters in sg-Ctrl (red) and *Nup210* KO (KO-N13) (blue) 4T1 cells.

(h) RNA-seq analysis showing the 2-fold up or downregulated genes upon knockdown of *Nup210* in 4T1 cells.

(i) Overlap of genes with 2-fold downregulation of H3K4me3 enrichment in *Nup210* KO 4T1 cells and 2-fold downregulated expression in *Nup210* knockdown 4T1 cells.

(j) Gene Ontology (GO) analysis of genes from the overlap of H3K4me3 ChIP-seq and RNA-seq analysis.

(k) Downregulated cell migration-related genes from the RNA-seq of 4T1 *Nup210* knockdown (sh-Nup # 4) cells. FC = fold change.

(l) Representative ChIP-seq track of *Cxcl* and *Ccl2* regions showing the association of NUP210-, H3K27Ac-, H3K27me3- and H3K4me3-enriched regions with predicted TADs. Publicly available Hi-C contact map from mESC data was used for TAD prediction.

(m) qRT-PCR analysis showing the downregulation of cell migration-related genes in both *Nup210* KO (KO-N13) vs sg-Ctrl and *Nup210* knockdown (sh-Nup # 4) vs sh-Ctrl 4T1 cells. *$P < 0.01$, **$P < 0.01$, ***$P < 0.001$, ****$P < 0.0001$.

(n) qRT-PCR analysis showing the expression of cell migration-related genes in DMSO- and GSK126-treated *Nup210* KO (KO-N13) 4T1 cells. **P < 0.01, ***P < 0.001, ****P < 0.0001, NS = non-significant.

(o) Representative super-resolution microscopy images showing H3.1/3.2 (green) and H3K27me3 distribution in DMSO- and GSK126-treated *Nup210* KO 4T1 cells. DNA is labeled with DAPI (blue). Scale bar = 5 μm.

(p) Quantification of the H3.1/3.2 fluorescence intensity ratio (nuclear periphery vs total) in DMSO- and GSK126-treated *Nup210* KO 4T1 cells. ****P < 0.0001. sg-Ctrl, n = 59; KO+DMSO, n = 79; KO+GSK126, n = 53.

(q) Quantification of the nuclear area in DMSO- and GSK126-treated *Nup210* KO 4T1 cells. ****P < 0.0001. n is the same as mentioned in (p).

Figure 6: NUP210 loss is associated with differential repositioning of mechanosensitive gene loci.

(a) Representative images of 3D-DNA FISH showing the position of NUP210-regulated gene loci (red) within the nucleus of 4T1 cells. DNA is labeled with DAPI (blue). Scale bar = 2 μm.

(b) Cumulative distribution of FISH spots in nuclear periphery vs nuclear centroid in sgCtrl (red) and *Nup210* KO (KO-N13) (blue) 4T1 cells. For the *Cxcl* region, sgCtrl n = 39, KO-N13 n = 78; for the *Postn* region, sgCtrl n = 94, KO-N13 n = 75; for the *Ccl2* region, sgCtrl n = 101, KO-N13 n = 80; for the *Itgb2* region, sgCtrl n = 37, KO-N13 n = 72.

(c) Minimum distance of FISH spots from heterochromatin foci (marked by strong DAPI signal) in sg-Ctrl and *Nup210* KO 4T1 cells. Number of cells (n) analyzed in each condition was the same as in (b).

Figure 7: *Nup210* is a mechanosensitive gene and regulates focal adhesion, cell migration, and invasion.

(a) Representative confocal images of focal adhesion puncta (marked by p-FAKY397 staining) in sh-Ctrl and *Nup210* knockdown (sh-Nup # 1 and # 4) 4T1 and 6DT1 cells. Scale bar = 10 μm.

(b) Quantification of focal adhesion puncta in sh-Ctrl and *Nup210* knockdown (sh-Nup # 1 and # 4) 4T1 and 6DT1 cells. ****$P < 0.0001$.

(c) Western blot showing the level of total FAK (T-FAK) and phospho-FAK (Y397) proteins in sh-Ctrl and *Nup210* knockdown (sh-Nup # 1 and # 4) T1 cells.

(d) Western blot showing the level of T-FAK and phospho-FAK (Y397) proteins in sh-Ctrl and *Nup210* knockdown (sh-Nup # 1 and # 4) 6DT1 cells.

(e) Representative images of 4T1 cells grown on fibronectin-coated hydrogel layers of different stiffness. Elastic modulus 0.2 kPa was used as a soft matrix and 12 kPa was used as a stiff matrix. Scale bar = 10 μm.

(f) Western blot analysis on whole cell lysate showing the NUP210, p-FAK Y397, and T-FAK protein levels when 4T1 cells were grown in soft (0.2 kPa) or stiff (12 kPa) conditions.

(g) qRT-PCR showing the differential expression of NUP210-regulated genes in soft (0.2 kPa) and stiff (12 kPa) matrices. *$P < 0.05$, **$P < 0.01$ and ***$P < 0.001$.

(h) Morphology of sh-Ctrl and *Nup210* knockdown (sh-Nup # 4) 4T1 cells in soft (0.2 kPa) and stiff (12 kPa) matrices. Scale bar = 10 μm.

(i) Representative images of F-actin stress fibers (phalloidin, green) after treatment and washout of cytochalasin D in sh-Ctrl and *Nup210* knockdown (sh-Nup # 4) 4T1 cells. DNA is labeled with DAPI (blue). Scale bar = 10 μm.

(j) Cell migration tracks (red) showing random migration of sg-Ctrl and NUP210 KO (KO-N9 and KO-N13) 4T1 cells (left). Quantification of cell speed is represented as a bar graph (right). ****$P < 0.0001$.

(k) Quantification (left) and representative images (right) of cell invasion for sg-Ctrl and *Nup210* KO (KO-N13) 4T1 cells. Percent cell invasion is quantified as total crystal violet intensity per transwell chamber. **$P < 0.01$, n = 3. Scale bar = 100 μm.

(l) Quantification (left) and representative images (right) of cell invasion for sh-Ctrl and *Nup210* knockdown (sh-Nup # 4) 6DT1 cells. *$P < 0.05$, n = 3. Scale bar = 100 μm.

Figure 8: NUP210 regulates a secretory phenotype that facilitates focal adhesion, cell migration *in vitro,* and circulating tumor cells in mice.

(a) Cytokine array on culture supernatants from sh-Ctrl and *Nup210* knockdown (sh-Nup # 4) 4T1 cells.

(b) Quantification of the cytokines/chemokines indicated on the array in (a).

(c) qRT-PCR analysis showing the knockdown of *Ccl2* in 4T1 cells.

(d) Western blot analysis showing the decrease of p-FAK Y397 protein without alteration of T-FAK in sh-Ctrl and *Ccl2* knockdown (sh-Ccl2 # 3, 4, and 5) 4T1 cells. β-actin was used as loading control.

(e) Focal adhesion puncta in sh-Ctrl and *Ccl2* knockdown (sh-Ccl2 # 5) 4T1 cells. Scale bar = 5 μm.

(f) Representative images (left) and quantification (right) of cell migration tracks (red) of sh-Ctrl and *Ccl2* knockdown (sh-Ccl2 # 3 and 5) 4T1 cells. ****P < 0.0001.

(g) Effect of *CCL2* amplification on overall survival of human breast cancer patients (METABRIC dataset).

(h) Flow cytometry analysis showing the percentage of CD45-/CK+ circulating tumor cells (CTCs) in mouse blood after orthotopic injection of sh-Ctrl or *Nup210* knockdown (sh-Nup # 4) 6DT1 cells. 6DT1 cells in culture were used to establish the CTC gate. Blood from healthy, tumor-free mice was used as negative control.

(i) Quantification of the percentage of CTCs from sh-Ctrl- and *Nup210* knockdown (sh-Nup # 4) 6DT1 cell-injected mice.

(j) Model depicting the proposed role of NUP210 in metastasis. In response to mechanical signals, NUP210 interacts with histone H3.1/3.2-associated poised chromatin at the nuclear pore and protects H3.1/3.2 from H3K27me3 heterochromatin modification. As a result, mechanosensitive, cell migration-related genes are activated to promote cell migration and metastasis. In the absence of NUP210, H3.1/3.2-associated chromatin undergoes heterochromatinization. Consequently, the mechanical signal cannot pass from the extracellular microenvironment to the nucleus to activate mechanosensitive gene expression, thereby decreasing metastasis.

SUPPLEMENTARY FIGURE LEGENDS:

Supplementary Figure 1: CTCF binding site in the *NUP210* promoter of a human breast cancer cell line, MCF7.

(a) Publicly available ChIP-seq tracks showing the enrichment of CTCF and H3K27Ac at the promoter of human *NUP210* in the MCF7 breast cancer cell line.

Supplementary Figure 2: Knockdown of *Nup210* in the 6DT1 and MVT1 cell lines decreases lung metastasis.

(a) Western blot showing the level of *Nup210* shRNA-mediated knockdown in 6DT1 cells (left) and qRT-PCR showing the *Nup210* knockdown level in MVT1 cells (right).

(b) Primary tumor weight after orthotopic transplantation of *Nup210* knockdown 6DT1 (left) or MVT1 (right) cells. ***P < 0.001, ****P < 0.0001

(c) Lung metastases count after orthotopic transplantation of *Nup210* knockdown 6DT1 (left) and MVT1 (right) cells. **P < 0.01, NS = non-significant.

(d) Lung metastases count normalized to primary tumor weight, derived from values shown in (b) and (c). *P < 0.05, **P < 0.01, ****P < 0.0001.

Supplementary Figure 3: Loss of NUP210 has a minor, inconsistent effect on cell cycle progression of 4T1 cells.

(a) DNA content analysis with EdU incorporation showing the different stages of the cell cycle in sg-Ctrl and *Nup210* KO (KO-N9 and KO-N13) 4T1cells.

(b) Quantification of cell cycle stage distribution in sg-Ctrl and *Nup210* KO (KO-N9 and KO-N13) 4T1 cells. *P < 0.05, **P < 0.01, n = 3.

Supplementary Figure 4: NUP210 loss does not affect general nucleocytoplasmic protein transport but may affect RNA transport.

(a) Schematic of the tdTomato-expressing nucleocytoplasmic transport reporter. Reporter expression is driven by a CMV promoter and produces tdTomato fused to both a nuclear export (NES) and import (NLS) signal.

(b) Representative immunofluorescence images showing nuclear and cytoplasmic localization of the tdTomato signal (red) in sh-Ctrl and *Nup210* knockdown (sh-Nup # 1 and 4) 4T1 cells. The Nuclear Pore Complex (NPC) is shown in green. Nuclei are stained with DAPI (blue). Leptomycin B, a nuclear export inhibitor drug, was used as positive control. Scale bar = 10 μm.

(c) (Left) Representative RNA FISH images showing the cytoplasmic and nuclear localization of PolyA+ RNA in sh-Ctrl and *Nup210* (sh-Nup # 1 and 4) knockdown 4T1 cells. Scale bar = 10 μm. (Right) Quantification of the nuclear FISH signal. ****$P < 0.0001$.

(d) (Left) Representative RNA FISH images showing the cytoplasmic and nuclear localization of PolyA+ RNA in sg-Ctrl and *Nup210* KO (KO-N9 and KO-N13) 4T1 cells. Scale bar 10 = μm. (Right) Quantification of the nuclear FISH signal. ****$P < 0.0001$.

Supplementary Figure 5: *Nup210* depletion in 4T1 (KO), MDA-MB-231 (KD), and MCF7 (KD) cells decreases focal adhesion kinase signaling.

(a) Representative immunofluorescence images showing focal adhesion in sg-Ctrl and *Nup210* KO (KO-N13) 4T1 cells. Scale bar = 10 μm.

(b) Western blot showing the protein levels of total focal adhesion kinase (T-FAK) and p-FAK Y397 in sg-Ctrl and *Nup210* KO (KO-N13) 4T1 cells.

(c) Western blot showing the protein levels of T-FAK and p-FAK Y397 in sh-Ctrl and *Nup210* knockdown MDA-MB-231 cells.

(d) Western blot showing the protein levels of T-FAK and p-FAK Y397 in sh-Ctrl and *Nup210* knockdown MCF7 cells.

METHODS:

CONTACT FOR REAGENT AND RESOURCE SHARING:

Further information and request for resources or reagents should be directed to and will be fulfilled by the lead contact, Kent W. Hunter (hunterk@mail.nih.gov).

EXPERIMENTAL MODELS AND SUBJECT DETAILS:

Mouse strains:

Usage of animals described in this study was performed under the animal study protocol LCBG-004 approved by the National Cancer Institute (NCI) at Bethesda Animal Use and Care Committee. Animal euthanasia was performed by anesthesia using Avertin injection followed by cervical dislocation. Female BALB/c (000651) and FVB/NJ (001800) mice were purchased from The Jackson Laboratory.

Cell lines:

Mouse mammary tumor cell lines, 4T07, 4T1, 6DT1, and MVT1, were provided by Dr. Lalage Wakefield (NCI, NIH)[34]. These cell lines were grown in DMEM (Gibco) supplemented with 9% fetal bovine serum (FBS) (Gemini), 1% L-glutamine (Gibco), and 1% penicillin-streptomycin (Gemini). Human breast cancer cell lines, MDA-MB-231 and MCF7, were provided by Dr. Jeffrey E. Green (NCI, NIH) and grown in DMEM with FBS, 1% L-glutamine, and 1% Penicillin-Streptomycin.

METHOD DETAILS:

Benzonase Accessible Chromatin (BACh) sequencing analysis:

Cells were expanded in DMEM at 37°C to obtain 8–10 x10^7 cells/condition/each experiment. BACh analysis was performed as previously described with minor modifications[94]. Briefly, cells were collected by centrifugation, washed twice in ice cold cellular wash buffer (20 mM Tris-HCl pH 7.5, 137 mM NaCl, 1 mM EDTA, 10 mM sodium butyrate, 10 mM sodium orthovanadate, 2 mM sodium fluoride, protease inhibitor cocktail (Roche) and resuspended in (40 million cells/ml) hypertonic lysis buffer (20 mM Tris-HCl pH 7.5, 2 mM EDTA, 1 mM EGTA, 0.5% glycerol, 20 mM sodium butyrate, 2 mM sodium orthovanadate, 4 mM sodium fluoride and protease inhibitor cocktail). Cells were distributed in 500 µl aliquots in 1.5 ml tubes and followed by the addition of 500 µl of nuclease digestion buffer (40 mM Tris-HCl pH 8.0, 6 mM $MgCl_2$, 0.3% NP-40, and 1% Glycerol) containing a 3-fold dilutions (from 0.125 units/ml to 6 units/ml) of Benzonase nuclease (Millipore). This was mixed gently and incubated for three minutes at 37°C. Reactions were terminated by the addition of EDTA (10 mM final concentration) and SDS (0.75% final concentration). Proteinase K was added to a final concentration of 0.5 mg/ml and incubated overnight at 45°C. DNA fragments of 100-500 bp from a chromatin digestion were purified over sucrose gradients[95] and precipitated in 0.1 volume sodium acetate and 0.7 volume isopropanol.

Sequencing and data analysis of Benzonase-treated samples:

DNA was sequenced using either Illumina HiSeq2000 (TrueSeq V3 chemistry) or NextSeq500 (TrueSeq High output V2 chemistry) sequencers at the Advanced Technology Research Facility (ATRF), National Cancer Institute (NCI-Frederick, MD, USA). The sequence reads were generated as either 50-mer or 75-mer (trimmed to 50-mer by trimmomatic software before

alignment), and tags are then aligned to the UCSC mm9 reference genome assembly using Eland or Bowtie2. All the samples were in good quality with over 94% of the bases having Q30 or above with 25~50 million raw reads per sample. Regions of enriched tags termed hotspots have been called using DNase2Hotspots algorithm[96] with FDR of 0% with minor updates. Tag density values were normalized to 10 million reads. For comparison of BACh profiles across multiple cell lines, Percent Reference peak Coverage (PRC) measure was proposed and employed to ensure compatible levels of digestion by Benzonase in multiple cell lines[97]. To calibrate PRC, commonly represented hotspot sites were identified as reference peaks based on mouse (mm9) DNaseq data from ENCODE. ENCODE narrowPeak definition files (DNaseI Hypersensitivity by Digital DNaseI from ENCODE/University of Washington) for a total of 133 samples were downloaded from the UCSC golden path web site: http://hgdownload.cse.ucsc.edu/goldenPath/mm9/encodeDCC/wgEncodeUwDnase/. A total of 8,587 peaks were found to be present in all 133 samples. By assuming that the most commonly accessible sites may also be present in our optimally digested samples, PRC was obtained as a fraction of reference peaks presented in each sample to evaluate the level of digestion by Benzonase. Our pooled samples with PRC of 90% or greater indicated that all the 8,587 sites were present in the sample. Two biological replicates with acceptable PRC were selected and pooled for each cell line, and each pooled data set showed over 90% PRC. When samples showed bimodality in their tag density distribution due to elevated noise, we dropped hotspots that belonged to a group with low tag density and low PRC by applying threshold to maximum hotspot tag density values.

Computing environment:

All computations at NCI were performed on the NIH helix/biowulf system, documentation of which is available at https://helix.nih.gov. We used the R computing environment, Perl scripts, Bedtools, and UCSC liftOver for most of the analyses.

Identification of polymorphic BACh sites:

The workflow consisted of the following: 1) the BACh data were filtered for the regions overlapping with polymorphic sites. Since the BACh data were generated in Genome Build mm9, we used UCSC mm9 snp128 data to restrict the BACh sites. 2) Variant Called Format (VCF) files were filtered to retain the SNPs that overlap with the BACh present in the 4T1 and 4T07 cell lines. 3) SNPs were removed in the BACh that are present in the mouse FVB/NJ strain.

Long Read Chromatin Interaction Analysis Through Paired-end Tag (ChIA-PET) sequencing and data processing

Long read ChIA-PET was performed using Tn5 transposase to tag DNA for long tag sequencing by Illumina NextSeq. ChIA-PET data was processed by a customized ChIA-PET data processing pipeline[29]. Detailed protocol can be found in Li et al.[98].

Cloning:

A mouse *Nup210* full length cDNA (NM_018815) encoding vector (pCMV6-Nup210-Myc) was purchased from Origene Technologies. This vector was digested with SalI-HF (New England Biolabs) and EcoRV-HF (New England Biolabs) restriction enzymes to obtain the NUP210 protein-encoding region. This NUP210 insert was then cloned into the Gateway entry vector

pENTR1A using the Quick Ligation Kit (New England Biolabs). pENTR1A no ccdB plasmid (Addgene plasmid # 17398) was received by Dr. Marian Darkin (NCI) as a gift from Dr. Eric Campeau. The NUP210-encoding region from the pCMV6-NUP210-Myc vector was cloned into pENTR1A vector through digestion with SalI and EcoRV. pENTR1A-NUP210 entry vector was used to transfer the NUP210-encoding region into the lentiviral destination vector pDEST-658 (received as a gift from Dr. Dominic Esposito, NIH) along with a mouse *Pol2* promoter entry vector using the Gateway LR clonase reaction (Thermo Fisher Scientific). The integrity of the final NUP210-encoding vector was verified through DNA sequencing.

The pGL4.23 [*luc2*/minP] promoter luciferase vector (Promega, Catalog # E8411) was received as a gift from Dr. Jing Huang (NCI, NIH). A 550 bp region from the mouse (FVB/NJ and BALB/cJ) *Nup210* promoter covering the polymorphic sites was amplified by PCR using KOD Hot Start DNA Polymerase (Millipore) and digested with KpnI (New England Biolabs) and XhoI (New England Biolabs) restriction enzymes. Gel-purified PCR product was then cloned into the pGL4.23 vector using T4 DNA ligase (New England Biolabs). Finally, the DNA sequence of the clones were confirmed through DNA sequencing.

Lentivirus production and generation of stable cell lines:

All of the TRC lentiviral shRNA vectors were purchased from Dharmacon. shRNAs targeting the mouse *Nup210* gene, sh-Nup # 1 (TRCN0000101935: TAACTATCACAGTAAGAAGGC) and sh-Nup # 4 (TRCN0000101938: TTCAGTTGCTTATCTGTCAGC) were used for *Nup210* knockdown in all of the mouse cell lines. For mouse *Ctcf* knockdown, sh-Ctcf # 4 (TRCN0000039022: TAAGGTGTGACATATCATCGG) and sh-Ctcf # 5 (TRCN0000039023:

ATCTTCGACCTGAATGATGGC) were used. For mouse *Ccl2* knockdown, sh-Ccl2 # 3 (TRCN0000034471: TTACGGGTCAACTTCACATTC), sh-Ccl2 # 4 (TRCN0000034472: TTGCTGGTGAATGAGTAGCAG), and sh-Ccl2 # 5 (TRCN0000034473: AATGTATGTCTGGACCCATTC were used. For *NUP210* knockdown in human cell lines, a shRNA targeting the human *NUP210* gene (TRCN0000156619: AAATGAGCTAATGGGCAGAGC) was used.

For lentivirus production, shRNA-containing plasmids and packaging plasmids, psPAX2 (Addgene plasmid # 12260) and envelope plasmid pMD2.G (Addgene plasmid # 12259) (both were a gift from the Trono lab), were transfected into the human 293FT (Thermo Fisher Scientific) cell line using X-tremeGENE 9 DNA transfection reagent (Roche). 48 h after transfection, culture supernatant containing lentivirus was harvested, filtered through a 0.45 μm filiter (Millipore), and then used for transduction of mouse and human breast cancer cell lines. shRNAs stably integrated in mouse and human cells were selected with 10 and 2 μg/ml puromycin (Sigma), respectively. For the selection of NUP210-overexpressing cells, 10 μg/ml of blasticidin (Gibco) was used.

CRISPR/Cas9-mediated knockout of the mouse Nup210 gene:

For CRISPR/Cas9-mediated knockout of mouse *Nup210* in the 4T1 cell line, sgRNA targeting *Nup210* exon 5 (sgRNA sequence: GCGACACCATCCTAGTGTCT) was designed using the GPP Web Portal available at the Broad Institute (https://portals.broadinstitute.org/gpp/public/analysis-tools/sgrna-design). sgRNA was then cloned into the lentiGuide-puro (Addgene plasmid # 52963, a gift from the Feng Zhang lab) vector. Non-targeting control sgRNA cloned into the lentiGuide-puro vector (sgRNA sequence: CCATATCGGGGCGAGACATG) was kind of a gift from Dr. Ji

Luo (NCI, NIH). Lentiviral particles were prepared as described above for shRNA lentiviruses. 4T1 cells stably expressing the sgRNAs were generated through lentiviral transduction and selection with 10 μg/ml puromycin. For transient expression of Cas9 in the sgRNA-stable 4T1 cells, an adenoviral Cas9-encoding viral particles containing the GFP reporter (Vector Biolab) was used at 25 M.O.I. 96 h after transfection of the Cas9 vector, GFP-positive 4T1 cells were FACS sorted and single cells were isolated for clonal expansion. *Nup210* mutation was confirmed through DNA sequencing and knockout was verified through western blot. Before performing functional assays with *Nup210* knockout cells, both sgCtrl and knockout cells were passaged at least 4 times for 2 weeks to eliminate residual Cas9-GFP signal within 4T1 cells, which was verified using a fluorescence microscope.

Spontaneous metastasis assay in mice:

6-8 weeks old female BALB/c and FVB/NJ mice were purchased from The Jackson Laboratory. For orthotopic transplantation of *Nup210*-depleted/overexpressing cells, 100,000 cells were injected into the fourth mammary fad pad of mice. 28-30 days after injection, mice were euthanized and primary tumors were resected, weighed, and surface lung metastases were counted.

Protein nucleocytoplasmic transport assay:

4T1 *Nup210* knockdown cells were grown on glass coverslips in 2-well Lab-Tek chambered glass coverslip (Thermo Fisher Scientific) at a seeding density of 20,000 cells/well. 24 h after seeding, cells were transfected with 1 μg of nucleocytoplasmic transport reporter (NLS-tdTomato-NES) plasmid (received as a gift from Dr. Martin W. Hetzer, Salk Institute) using Novagen Nanojuice Transfection Reagent (Millipore-Sigma). 4 h after transfection, medium was replaced with fresh

medium and cells were grown for 24 h. Cells were then treated with 20 nM leptomycin B (Cell Signaling Technology) for 6 h and then fixed with methanol for immunostaining with an antibody against nuclear pore complex proteins (clone mAb414, Abcam) following the regular immunofluorescence protocol described below. Nuclear and cytoplasmic expression of tdTomato was observed using confocal microscopy.

RNA export assay using Oligo-d(T) Fluorescence In situ Hybridization (FISH):

Oligo-dT RNA FISH analysis was performed as described elsewhere (https://openwetware.org/wiki/Poly_A_RNA_in_situ_protocol). Briefly, *Nup210* knockdown and knockout cells were seeded in 4-well μ-Slides (Ibidi) at a seeding density of 100,000 cells/well. After 24 h of incubation, cells were fixed with 4% paraformaldehyde for 10 min followed by 100% ice-cold methanol and 70% ethanol. Cells were then incubated with 1M Tris-HCl pH 8.0 for 5 min. 1 ng/ml 5'-Cy3-Oligo d(T)50 probe (Gene Link) mixed with hybridization buffer (1 mg/ml yeast tRNA, 0.005% BSA, 10% dextran sulfate, 25% deionized formamide, and 2X SSC buffer) was added on to cells and incubated at 37°C in a humidified chamber for 1 h. After hybridization, cells were washed with 4X SSC and 2X SSC buffer. Cells were then incubated with 1 μg/ml DAPI in 2X SSC containing 0.1% Triton X-100 for 15 min. After washing with 2X SSC, images were captured using a Zeiss LSM 880 Airyscan confocal microscope. Nuclear Oligo-d(T) signal intensity was quantified using the Image-Pro Premier (Media Cybernetics) software.

Protein interaction analysis through Liquid Chromatography-Mass Spectrometry (LC-MS):

NUP210-Myc overexpressing 4T1 cells were seeded onto 15 cm tissue culture dishes at a seeding density of 2.5×10^6 cells/dish. After 48 h of incubation, cells were harvested and nuclear protein

complex lysates were prepared using the Nuclear Complex Co-IP Kit (Active Motif). Co-immunoprecipitation with two biological replicates was performed according to the manufacturer's instructions. Briefly, 500 μg of nuclear protein lysates were incubated with 2 μg of either Myc-Tag antibody (Cell Signaling Technology) or an endogenous NUP210-specific antibody (Bethyl Laboratories). After overnight incubation on a rotator at 4°C, 25 μg of Dynabeads Protein G (Invitrogen) were added to the protein lysate-antibody complexes. After 30 min of incubation with beads, antibody-bead-protein complexes were isolated using a magnetic stand. Beads were then washed three times and then dissolved in 25 mM ammonium bicarbonate pH 8.0 (Sigma). Samples were then subjected to LC-MS analysis.

Western blot:

Whole cell protein lysate was prepared using lysis buffer (20 mM Tris-HCl pH 8.0, 400 mM NaCl, 5 mM EDTA, 1 mM EGTA, 10 mM NaF, 1 mM sodium pyrophosphate, 1% Triton X-100, 10% glycerol, protease and phosphatase inhibitor cocktail). Nuclear and cytoplasmic protein lysates were prepared using the Nuclear Extract Kit (Active Motif) or Nuclear Complex Co-IP Kit (Active Motif). Protein concentration was measured using the Pierce BCA Protein Assay Kit (Thermo Fisher Scientific). 25 μg of protein lysates were mixed with 4x NuPAGE LDS sample buffer (Invitrogen) and 10x NuPAGE Sample Reducing Agent (Invitrogen). Samples were then boiled at 95°C for 5 min and resolved on NuPAGE 3-8% Tris-acetate, NuPAGE 4-12% Bis-Tris, or Novex 4-20% Tris-Glycine protein gels (Thermo Fisher Scientific) with appropriate running buffer. Protein was transferred onto a PVDF membrane (Millipore) and the membrane was blocked with blocking buffer (TBST + 5% Non-fat dry milk) for 1 h. Membranes were then incubated with appropriate primary antibodies overnight. After washing with TBST, membranes were incubated

with secondary antibodies for 1 h. Finally, the signal was developed on X-ray film using the Amersham ECL Western Blotting Detection Reagent (GE Healthcare).

Primary antibodies and their dilutions were as follows: NUP210 (1:500; Bethyl Laboratories), β-actin (1:10,000; Abcam), Lamin B1 (1:5,000; Abcam), Myc-Tag (1:1,000; Cell Signaling Technology), SUN2 (1:1,000; Abcam), FAK (1:5,000; Abcam), p-FAK(Y397) (1: 5,000; Abcam), H3.1/3.2 (1:1,000; Active Motif), H3K27me3 (1:5,000; Cell Signaling Technology), H3K9me3 (1:5,000; Abcam), SUV39H1 (1:1,000, Cell Signaling Technology), EZH2 (1:1,000; Cell Signaling Technology), and SUZ12 (1:1,000; Cell Signaling Technology). Anti-mouse secondary antibody (GE Healthcare) was used at 1:10,000 dilution and anti-rabbit secondary antibody (Cell Signaling Technology) was used at 1:3,000 dilution.

Co-immunoprecipitation:

Co-immunoprecipitiation was performed using the Nuclear Complex Co-IP Kit (Active Motif). 4T1 cells were seeded onto 15 cm tissue culture dishes at a seeding density of $5x10^6$ cells/dish. After 48 h of incubation, cells were harvested and nuclear lysates were prepared. 200-500 μg of nuclear lysates were incubated with 2 μg of specific antibodies and 50 μg of Dynabeads Protein G (Invitrogen). After overnight incubation on a rotator at 4°C, immune complexes were isolated using a magnetic stand. Beads were then washed three times, resuspended in 2x NuPAGE LDS sample buffer (Invitrogen), and incubated at 95°C heat block for 5 min. Samples were loaded onto NuPAGE protein gels and the standard western blot protocol was followed as described above.

Immunofluorescence and confocal microscopy:

Immunofluorescence analysis was performed as described previously[36]. Briefly, cells were grown on 4-well or 8-well polymer coverslips (Ibidi) at a seeding density of 40,000 or 20,000 cells/well, respectively. After 24 h of incubation, cells were fixed with -20°C methanol for 2 min and permeabilizaed with PBS containing 1% Triton X-100 for 1 min. Fixed cells were then blocked with immunofluorescence buffer (1x PBS, 10 mg/ml BSA, 0.02% SDS, and 0.1% Triton X-100) for 30 min. Cells were then incubated with primary antibodies diluted in immunofluorescence buffer overnight at 4°C. After washing the cells with immunofluorescence buffer three times for 10 min per wash, cells were incubated with Alexa Fluor-conjugated secondary antibodies for 1 h at room temperature. Cells were washed three times with immunofluorescence buffer and then incubated with 1 μg/ml DAPI (4′,6-diamidino-2-phenylindole) for 10 min to stain the nucleus. After washing the cells with PBS three times, slides were kept at 4°C until subjected to confocal microscopy. Images were acquired using either a Zeiss LSM 780 confocal microscope (63x plan-apochromat N.A. 1.4 oil immersion objective lens, 0.09 μm X-Y pixel size and 1.0 μm optical slice thickness), a Zeiss LSM 880 Airyscan super-resolution microscope (Airyscan detector, 63x plan-apochromat N.A. 1.4 oil immersion objective lens and 0.05 μm X-Y pixel size) or a Nikon SoRa spinning disk super-resolution microscope (Yokogawa SoRa spinning disk unit, 60x plan-apochromat N.A. 1.49 oil immersion objective lens, Photometrics BSI sCMOS camera, and 0.027 μm X-Y pixel size). Airyscan images were processed using the Airyscan processing algorithm in the Zeiss ZEN Black (v.2.3) software, whereas the Nikon SoRa images were deconvolved using a constrained iterative restoration algorithm in the Nikon NIS Elements (v5.11) software. Tetraspeck 0.2 μm beads (Invitrogen) were imaged with the same microscope parameters and used for channel alignment.

Primary antibodies used for immunofluorescence were as follows: p-FAK (Y397) (1:100; Abcam), H3.1/3.2 (1:1,000; Active Motif), mouse Myc-Tag (1:500; Cell Signaling Technology), rabbit Myc-Tag (1:100; Cell Signaling Technology), rabbit H3K27me3 (1:1,000), mouse H3K27me3 (1:250; Abcam), H3K9me3 (1:1,000; Abcam), Nucleolin (1:500; Abcam), and Nuclear Pore Complex (NPC) antibody (clone mAb414, 1:1,000; Abcam). Secondary antibodies used were mouse Alexa Fluor 488 (1:200; Invitrogen), rabbit Alexa Fluor 488 (1:200; Invitrogen), rabbit Alexa Fluor 568 (1:200; Invitrogen), rabbit Alexa Fluor 594 (1:200; Invitrogen), and mouse Alexa Fluor 594 (1:200).

Cell cycle analysis:

Cell cycle analysis was performed using the Click-iT EdU Alexa Fluor 488 Flow Cytometry Assay Kit (Thermo Fisher Scientific) and FxCycle Violet Stain (Thermo Fisher Scientific) according to manufacturer's instructions. Briefly, 4T1 cells were seeded onto 15 cm tissue culture dishes at a seeding density of $3x10^6$ cells/dish. 24 h later, cells were pulsed with Click-iT EdU (5-ethynyl-2´-deoxyuridine) for 1 h. After harvesting the cells through trypsinization, cells were fixed with Click-iT fixative and permeabilized with saponin-based permeabilization agent. The Click-iT reaction was then performed for 30 min at room temperature. Cells were then washed with wash buffer and stained for DNA content analysis with FxCycle Violet, a DNA-selective dye. Finally, cell cycle analysis was performed using a BD FACSCanto II flow cytometer (BD Bioscience). Data was analyzed using FlowJo V10 (FlowJo, LLC) software.

Chromatin immunoprecipitation followed by sequencing (ChIP-seq) analysis:

Chromatin immunoprecipitation (ChIP) was carried out using the ChIP-IT Express Enzymatic Chromatin Immunoprecipitation Kit (Active Motif) according to manufacturer's instructions. Briefly, $5x10^6$ 4T1 cells were seeded onto 15 cm tissue culture dishes. After 48 h of incubation, cells were fixed with 1% formaldehyde for 10 min at room temperature. Cells were washed with ice-cold PBS and formaldehyde cross-linking was quenched using glycine stop-fix solution. Cells were harvested through scraping and pelleted by centrifugation at 2,500 rpm for 10 min at 4°C. After cell lysis with ice-cold lysis buffer and a dounce homogenizer, chromatin was sheared using an enzymatic shearing cocktail for 12 min at 37°C. The shearing reaction was stopped with 0.5 M EDTA and the chromatin was separated through centrifugation at 15,000 rpm for 10 min at 4°C. 60-70 μg of chromatin were used with 25 μl of Protein G magnetic beads and 2 μg of specific antibodies for each ChIP reaction. The following antibodies were used for the ChIP reactions: anti-rabbit NUP210 (Bethyl Laboratories), anti-rabbit H3K27me3 (Cell Signaling Technology), anti-rabbit H3K4me3 (Millipore), and anti-mouse Nuclear Pore Complex (NPC) antibody (clone mAb414, Abcam). After incubating the reaction mixture overnight at 4°C on a rotator, the beads were washed with ChIP buffers and DNA was eluted with elution buffer. DNA was then reverse-cross linked, proteinase K-treated, and DNA quality was assessed using a Agilent Bioanalyzer before ChIP-seq library preparation. The library was prepared using a TruSeq ChIP Library Preparation Kit (Illumina) and pooled samples were sequenced on the NextSeq platform.

ChIP-seq data was analyzed using the Sicer algorithm[45] with default parameters. For narrow peaks such as H3K4me3 enrichment, a window size of 200 was used. For broad peaks such as H3K27me3 and NUP210, a window size of 1000 was used. The ChIP-seq plot profile was

generated using deepTools2[99]. For ChIP-seq peak annotation, the ChIPSeeker[100] Bioconductor package was used. BigWig files were displayed using the Integrative Genomics Viewer (IGV)[101].

Publicly available ChIP-seq and Hi-C data analysis:

H3K27Ac ChIP-seq data from mouse mammary luminal cells were downloaded from Gene Expression Omnibus (GEO) (Accession No: GSE116384)[34]. CTCF ChIP-seq data from mouse mammary epithelial cells were obtained from GEO (Accession No: GSE92587, sample: GSM2433042)[26]. CTCF and H3K27Ac ChIP-seq data from the MCF7 human breast cancer cell line were obtained from GEO (Accession No: GSE130852). Publicly available Hi-C data from mouse embryonic stem cells were derived from Bonev et al.[48] and displayed using the 3D Genome Browser[49].

RNA isolation and quantitative reverse transcriptase real-time PCR (qRT-PCR):

Cells were directly lysed on cell cultures plate with 1 ml TriPure Isolation Reagent (Sigma). After adding 200 µl chloroform and centrifuging at 14,000 rpm for 15 min at 4°C, the upper aqueous layer containing the RNA was transferred to new tube. To precipitate RNA, 500 µl of isopropanol was added to each tube, which was then vortexted and incubated at -20°C for 1 h. The RNA was further purified using the RNeasy Mini Kit (Qiagen) with on-column DNase (Qiagen) digestion according to manufacturer's instructions. 2 µg of total RNA was used for cDNA preparation using the iScript cDNA synthesis kit (Bio-Rad). A 1/10 dilution of cDNA was used for qRT-PCR analysis using the FastStart Universal SYBR Green Master Mix (Roche). Sequences of the primers used are listed in the reagents or resource table.

ChIP qPCR analysis:

Chromatin was isolated from 4T1 and 6DT1 cells using the ChIP-IT Express Enzymatic kit (Active Motif) according to manufacturers's instructions as mentioned above. 10 µl of normal rabbit IgG (Cell Signaling Technology), 10 µl of rabbit CTCF (Cell Signaling Technology), and 10 µl of rabbit H3K27Ac (Cell Signaling Technology) antibodies were used for the immunoprecipitation reaction. ChIP DNA was then subjected to qPCR analysis. The percent (%) input method was used for the calculation of CTCF and H3K27Ac enrichment.

RNA-seq analysis:

4T1 cells were seeded onto 6 cm tissue culture dishes at a seeding density of $4x10^5$ cells/dish. After 48 h of incubation, total RNA was isolated using the protocol described above. On-column DNase treatment was performed to eliminate DNA contamination. Library preparation was performed using the TruSeq Stranded mRNA Library Prep Kit (Illumina) and pooled samples were sequenced on a HiSeq2500 with TruSeq V4 chemistry (Illumina). Differential gene expression analysis from RNA-seq data was performed using Partek Flow software. Gene ontology (GO) enrichment analysis of differentially expressed genes was performed using the PANTHER classification system [102].

Promoter luciferase assay:

24-well tissue culture plates were coated overnight with 100 µg/ml type I collagen. 293FT cells were seeded in antibiotic free medium at a seeding density of 75,000 cells/well of 24-well plate. 250 ng of pGL4.23 *Nup210* luciferase promoter vectors and 25 ng of pRL-TK renilla luciferase vectors were co-transfected using NanoJuice transfection reagent (Millipore). 24 h after

transfection, the luciferase assay was performed using Dual-Luciferase Reporter Assay System kit (Promega) according to the manufacturer's instructions. Luciferase activity was measured using a GloMax 96 Microplate Luminometer (Promega). Firefly luciferase activity was normalized with Renilla luciferase activity. Eight biological replicates were used per condition.

Cytokine array:

4T1 *Nup210* knockdown cells were cultured in low serum condition (1% FBS) in 6-well plates at a seeding density of 500,000 cells per well. 24 h after incubation, cell culture supernatants were harvested and centrifuged to remove the dead cells. 1 ml of supernatant was used for cytokine profiling using the Proteome Profiler Mouse XL Cytokine Array (R & D Biosystems) according to manufacturer's instructions. Chemiluminescent signals were quantified using ImageJ (NIH) software.

3D DNA FISH analysis:

For DNA FISH analysis, cells were grown on Lab-Tek chamber slides. Cells were briefly washed with PBS and fixed with 4% paraformaldehyde. Cells were permeabilized with 0.2% Triton X-100 in PBS and then hybridized with labeled probe. For probe generation, BAC clones were purchased from CHORI (https://bacpacresources.org/). The following BAC clones were used for the experiment: *Cxcl* region: clone RP23-374O6; *Postn* region: clone RP23-480C1; *Ccl2* region: clone RP23-99N1, and *Itgb2* region: clone RP23-166E21. All the clones were expanded and DNA was isolated using the FosmidMax DNA Purification Kit (Epicentre). DNA from each clone was labeled through nick translation with either the Atto550 NT Labeling Kit (Jena Bioscience) or the Digoxigenin NT Labeling Kit (Jena Bioscience). Hybridization was carried out in a humidified

chamber at 37°C for 16 h. Post-hybridization rapid wash was carried out with 0.4x SSC at 72°C for 4 min. Digoxigenin was detected with a DyLight 594-Labeled Anti-Digoxigenin/Digoxin (DIG) antibody (Vector Laboratories). The slides were stained with DAPI and Z-stack images were captured using a Zeiss LSM880 Airyscan microscope.

Mechanotransduction assay:

To test the mechanotransduction effect, polyacrylamide hydrogel-bound cell culture plates with different elastic moduli was used as a mimic of extracellular matrix (ECM) stiffness. 6-well plates with 0.2 kPa (soft) or 12 kPa (stiff) elastic moduli were purchased from Matrigen. Each well of the plate was coated with 20 μg/ml fibronectin (Sigma) in PBS for 1 h at 37°C. After washing the well with PBS, 4T1 cells were seeded on top of soft or stiff matrix at a seeding density of 100,000 cells/well. 48 h after incubation, cells were harvested for RNA or protein isolation.

Focal adhesion assay:

For focal adhesion immunostaining, Lab-Tek 2-well glass chamber slides (Thermo Fisher Scientific) were coated with 50 μg/ml of collagen type I matrix (Gibco) and cells were seeded at a seeding density of 20,000 cells/well. After overnight incubation, cells were fixed in 4% paraformaldehyde for 20 min. Cells were then washed with PBS, permeabilized with PBS + 0.1% Triton X-100 for 5 min, and blocked with PBS + 5% normal goat serum. Cells were incubated with phospho-FAK (Y397) antibody for 1 h. After washing with PBS, cells were incubated with Alexa Fluor 594-conjugated rabbit secondary antibody and Alexa Fluor 488-conjugated phalloidin (F-actin staining) for 1 h. The slides were then washed with PBS and mounted using VECTASHIELD with DAPI Mounting Medium (Vector Laboratories). Images were captured

using a Zeiss 780/880 confocal microscope and automated counting of focal adhesion puncta (phospho-FAK staining) was performed using Image-Pro Plus software (Media Cybernetics).

Actin polymerization inhibition assay using cytochalasin D:

For the cytochalasin D treatment of 4T1 *Nup210* knockdown cells, 20,000 cells were seed onto 4-well μ-Slides with polymer coverslips (Ibidi). 24 h later, cells were treated with 1 μM cytochalasin D, a potent inhibitor actin polymerization, for 2 h. After the treatment, cells were washed with complete medium three times and incubated for another 2 h in a 37°C CO_2 incubator for the recovery of actin polymerization. Cells were then fixed with 4% paraformaldehyde for 30 min and stained with Alexa Fluor 488-conjugated phalloidin for immunofluorescence imaging. Nuclei were stained with 1 μg/ml Hoechst 33342 (Thermo Fisher).

EZH2 inhibitor (GSK126) treatment:

For immunofluorescence microscopy, 4T1 sg-Ctrl and *Nup210* KO cells were seeded onto 4-well μ-Slides at a seeding density of 25,000 cells/well. 24 h later, KO cells were treated with either DMSO or 5 μM GSK126 (Selleckchem) for another 24 h. Cells were then fixed with -20°C methanol for 2 min. Histone H3.1/3.2 and H3K27me3 antibodies were used for immunofluorescence staining according to the protocol described above[36].

For the qRT-PCR analysis, $2x10^5$ 4T1 *Nup210* KO cells were seeded onto 6 cm dishes. 24 h later, 5 μM GSK126 was applied to the cells that were then incubated for another 48 h. Cells were then lysed, RNA was isolated, and qRT-PCR was performed as described above.

Cell migration assay:

For the automated random cell migration assay, 4T1 cells were seeded onto 96-well polystyrene microplates (Corning) at a seeding density of 2,000 cells/well so that the cell density remained sub-confluent until the end of the imaging period. After 24 h of incubation, cells were incubated with complete medium containing 200 ng/ml Hoechst 33342 (Thermo Fisher Scientific) for 1 h. Cells were then transferred to a Nikon Eclipse Ti2 microscope. Images were captured every 12 minutes with a 20x 0.8 NA objective for 24 h. Total light exposure time was kept to 200 milliseconds for each time point. Cells were imaged in a humidified 37°C incubator with 5% CO_2. Image processing and cell tracking were carried out with custom MATLAB script described previously[103].

Cell invasion assay:

The cell invasion assay was performed using BioCoat Matrigel Invasion Chambers with 8.0 µm PET Membrane (Corning) according to manufacturer's instructions. Briefly, 7.5×10^5 4T1 and 6DT1 cells were seeded onto the top well containing DMEM with 0.5% serum. In the bottom well, DMEM with 10% serum was used as a chemoattractant. Cells were incubated in a 37°C incubator for 24 h and 48 h for 6DT1 and 4T1 cells, respectively. After incubation, non-invaded cells were removed from the top well using cotton tips. Cells that had invaded into the Matrigel were then fixed with methanol and stained with 0.05% crystal violet. Matrigel membranes containing invaded cells were then cut and mounted onto glass slides with Vectashield mounting medium (Vector Laboratories). Images of entire membranes were captured as segments and then stitched using an EVOS FL Auto 2 microscope (Invitrogen). Image analysis was performed using Image-

Pro Premier 3D (Media Cybernetics) software. Percent cell invasion was calculated using crystal violet intensity per membrane area.

Circulating tumor cell (CTC) analysis:

100,000 6DT1 cells with or without *Nup210* knockdown were injected into the fourth mammary fat pad of FVB/NJ mice. Ten mice were used in each group and three mice were kept uninjected for use as healthy controls. One month after injection, mice were anesthetized with avertin injection. Through cardiac puncture, 600-1000 μl blood per mouse was collected in 50 μl of 0.5 M EDTA solution. An equal volume of blood was taken for red blood cell lysis using ACK lysis buffer. 100 μl of the peripheral blood lymphocyte (PBL) fraction was subjected to fixation with 2% paraformaldehyde for 15 min at room temperature. Cells were permeabilized with PBS containing 0.1% Triton X-100. Cells were vortexed briefly and kept at room temperature for 30 min. 0.5% BSA in PBS was added and cells were pelleted by centrifugation. Cells were then resuspended in ice-cold 50% methanol in PBS and incubated for 10 min on ice. 150,000 fixed cells were stained for CD45, a pan-lymphocyte marker, and pan-keratin, a tumor cell marker. Before staining with antibodies, cells were incubated with FcR Blocking Reagent (1:10 dilution; Miltenyi) for 10 min at 4°C. Cells were then stained with APC-conjugated CD45 (1:25 dilution; Miltenyi) and Alexa Fluor 488-conjugated pan-keratin (1:25 dilution, Cell Signaling Technology) antibodies for 10 min at 4°C. After washing with MACS buffer (PBS, 0.5% BSA, and 2 mM EDTA), cells were incubated with 1 μg/ml Hoechst 33342 (Thermo Fisher Scientific) for 5 min. Cells were then washed again with MACS buffer and resuspended in 200 μl buffer for analysis using a BD FACSCanto II flow cytometer. A CTC (CD45-/Cytokeratin+) gate was created based on the

staining pattern of 6DT1 tumor cells in culture and primary tumor cells derived from 6DT1-injected mice. Flow cytometry data was analyzed using FlowJo V10 software.

Patient datasets analysis:

Distant metastasis-free survival analysis on gene expression signature was performed using GOBO tool (http://co.bmc.lu.se/gobo/gobo.pl)[104]. Data on *NUP210* and *CCL2* amplification in human breast cancer patients was derived from Molecular Taxonomy of Breast Cancer International Consortium (METABRIC) data available on cBioPortal (https://www.cbioportal.org/)[105]. METABRIC NUP210 mRNA expression data was also downloaded from the cBioPortal database and manually processed for further analysis. Distant metastasis-free survival data was obtained from the Km-plotter database (https://kmplot.com/analysis/). The JetSet best probe 213947_s_at was used for *NUP210* expression and patients were separated by upper and lower quartile values. *NUP210* gene expression data on breast cancer metastatic sites, prostate cancer and melanoma were downloaded from Gene Expression Omnibus (GEO).

QUANTIFICATION AND STATISTICAL ANALYSIS:

Statistical analysis:

In case of the *in vivo* animal studies, p-values were calculated using the Mann-Whitney test in GraphPad Prism 8 software and the results were reported as mean ± standard deviation. For qRT-PCR result analysis, p-values were calculated using a two-tailed, unpaired t-test in GraphPad Prism and results were reported as mean ± standard error of mean (s.e.m).

Microscopy image analysis and quantification:

The periphery/total nuclear area intensity ratio of histone H3.1/3.2, H3K27me3, and H3K9me3 was quantified using Fiji software [106]. Briefly, total nuclear area was defined by DAPI staining, while the nuclear periphery was defined as the region 25% towards the interior from the nuclear edge (average distance for sg-Ctrl: 0.97 μm and KO-N13: 0.89 μm). Mean fluorescence intensity was quantified in both the periphery and total nuclear area and the periphery/total ratio was plotted. The heterochromatic foci/total nuclear area intensity of histone H3.1/3.2 was quantified using Fiji software. Heterochromatic foci regions were segmented using DAPI staining. Mean fluorescence intensity was quantified in both heterochromatic foci and total nuclear area and the heterochromatic foci/total ratio was plotted as box plots (bottom and top of the box denote first and third quartile respectively, whiskers denote -/+ 1.5 interquartile range (IQR), horizontal lines denote median values). p-values were calculated using a two-tailed Mann-Whitney U-test.

The position of DNA FISH spots relative to the nuclear centroid and periphery was quantified using the Cell module within the Imaris image analysis suite (Bitplane). To account for differences in nuclear size, the relative position was calculated by dividing the shortest distance of the FISH spot to the nuclear centroid, by the length of the three-point line encompassing the nuclear centroid, FISH spot, and nuclear periphery. Relative positions were plotted as cumulative distribution frequencies using RStudio software. p-values were calculated using a two-tailed Mann-Whitney U-test. The distance of DNA FISH spots to heterochromatic foci was quantified using Fiji software with the 3D region of interest (ROI) manager plugin, TANGO[107]. Heterochromatic foci were segmented using DAPI staining and used to create a distance map. DNA FISH spots were segmented and the distance to the nearest heterochromatic foci was calculated and plotted as box

plots (bottom and top of the box denote first and third quartile respectively, whiskers denote -/+ 1.5 interquartile range (IQR), horizontal lines denote median values). p-values were calculated using a two-tailed Mann-Whitney U-test.

DATA AND SOFTWARE AVAILABILITY:

Gene expression data will be deposited in Gene Expression Omnibus (GEO) prior to publication.

Figure 1

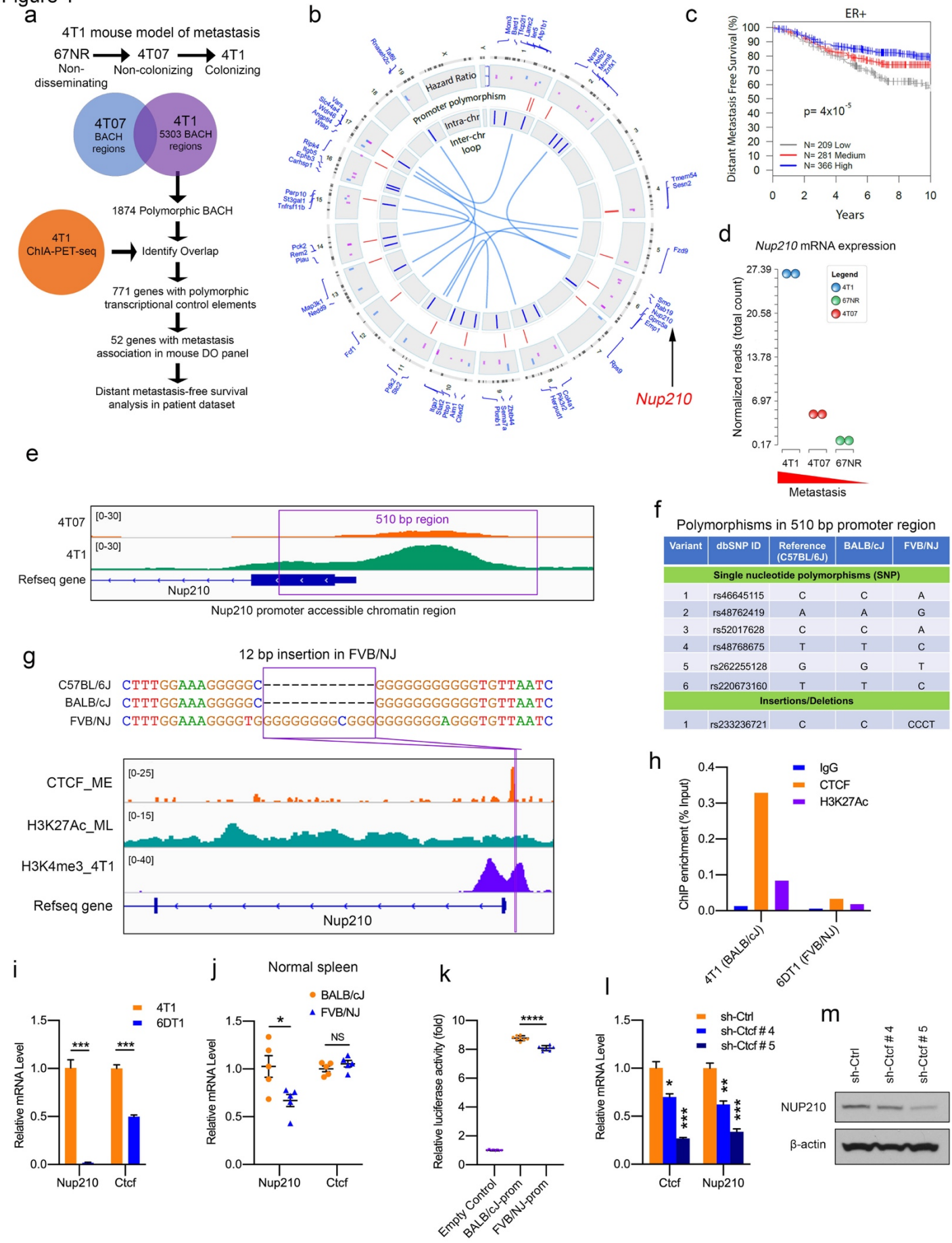

Variant	dbSNP ID	Reference (C57BL/6J)	BALB/cJ	FVB/NJ
Single nucleotide polymorphisms (SNP)				
1	rs46645115	C	C	A
2	rs48762419	A	A	G
3	rs52017628	C	C	A
4	rs48768675	T	T	C
5	rs262255128	G	G	T
6	rs220673160	T	T	C
Insertions/Deletions				
1	rs233236721	C	C	CCCT

Figure 2

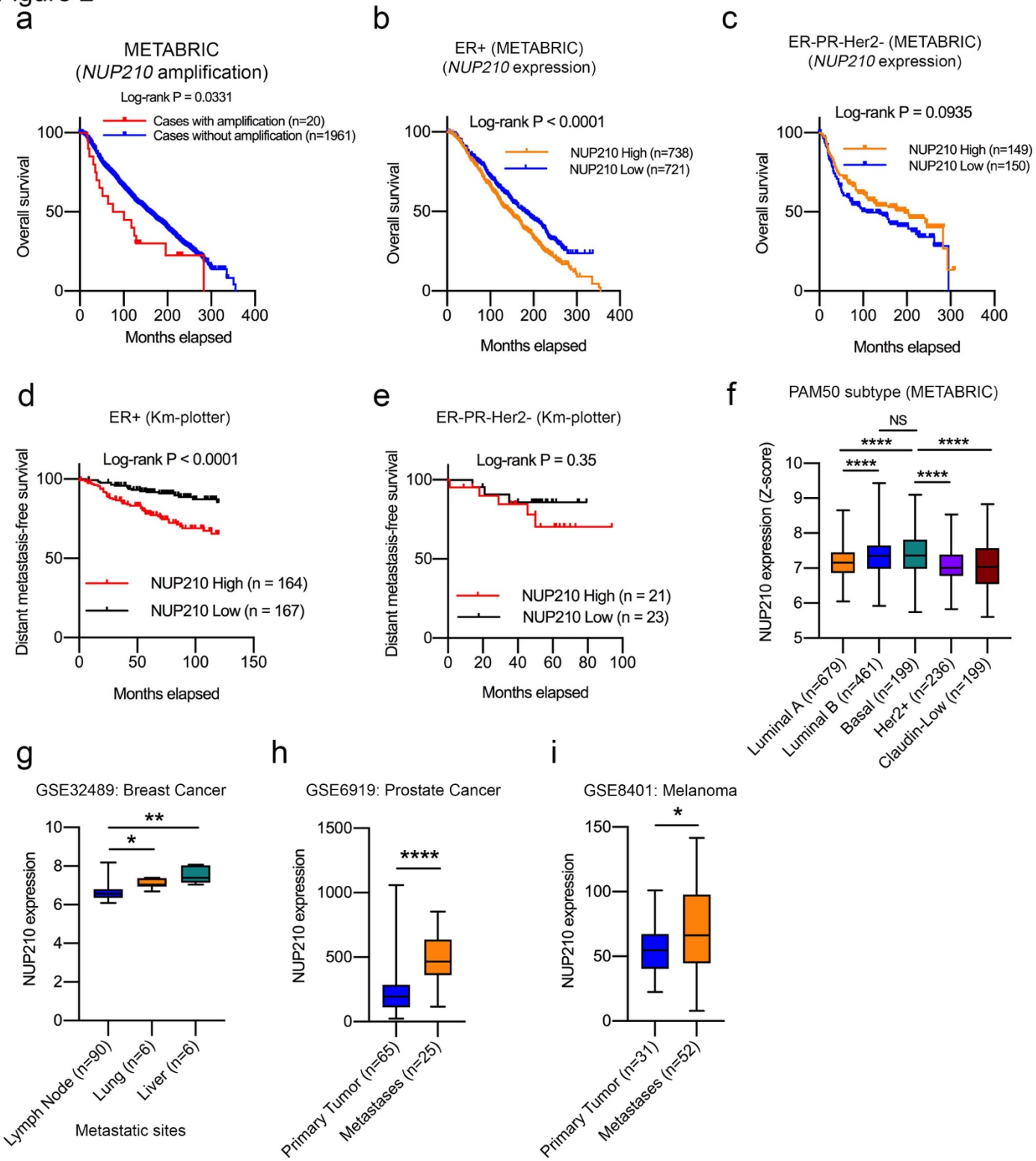
a
METABRIC
(NUP210 amplification)
Log-rank P = 0.0331
Cases with amplification (n=20)
Cases without amplification (n=1961)
Overall survival
Months elapsed
b
ER+ (METABRIC)
(NUP210 expression)
Log-rank P < 0.0001
NUP210 High (n=738)
NUP210 Low (n=721)
Overall survival
Months elapsed
c
ER-PR-Her2- (METABRIC)
(NUP210 expression)
Log-rank P = 0.0935
NUP210 High (n=149)
NUP210 Low (n=150)
Overall survival
Months elapsed
d
ER+ (Km-plotter)
Log-rank P < 0.0001
NUP210 High (n = 164)
NUP210 Low (n = 167)
Distant metastasis-free survival
Months elapsed
e
ER-PR-Her2- (Km-plotter)
Log-rank P = 0.35
NUP210 High (n = 21)
NUP210 Low (n = 23)
Distant metastasis-free survival
Months elapsed
f
PAM50 subtype (METABRIC)
NS
****
****
****
****
NUP210 expression (Z-score)
Luminal A (n=679)
Luminal B (n=461)
Basal (n=199)
Her2+ (n=236)
Claudin-Low (n=199)
g
GSE32489: Breast Cancer
**
*
NUP210 expression
Lymph Node (n=90)
Lung (n=6)
Liver (n=6)
Metastatic sites
h
GSE6919: Prostate Cancer
****
NUP210 expression
Primary Tumor (n=65)
Metastases (n=25)
i
GSE8401: Melanoma
*
NUP210 expression
Primary Tumor (n=31)
Metastases (n=52)

Figure 3

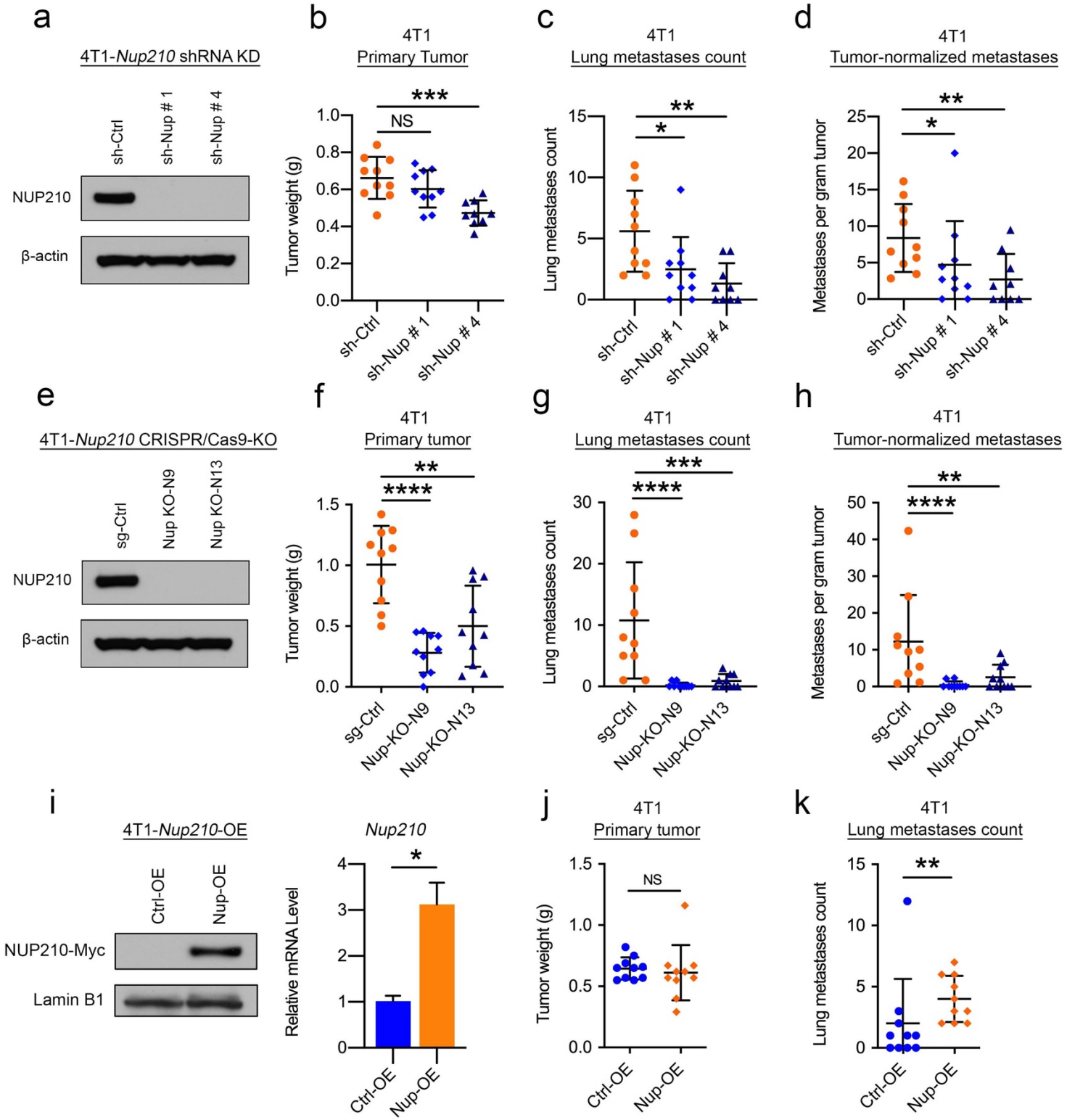
a
4T1-Nup210 shRNA KD
sh-Ctrl
sh-Nup # 1
sh-Nup # 4
NUP210
β-actin
b
4T1
Primary Tumor
Tumor weight (g)
NS
***
sh-Ctrl
sh-Nup # 1
sh-Nup # 4
c
4T1
Lung metastases count
Lung metastases count
**
*
d
4T1
Tumor-normalized metastases
Metastases per gram tumor
**
*
e
4T1-Nup210 CRISPR/Cas9-KO
sg-Ctrl
Nup KO-N9
Nup KO-N13
NUP210
β-actin
f
4T1
Primary tumor
Tumor weight (g)
**
****
sg-Ctrl
Nup-KO-N9
Nup-KO-N13
g
4T1
Lung metastases count
Lung metastases count
***
****
h
4T1
Tumor-normalized metastases
Metastases per gram tumor
**
****
i
4T1-Nup210-OE
Ctrl-OE
Nup-OE
NUP210-Myc
Lamin B1
Nup210
Relative mRNA Level
*
j
4T1
Primary tumor
Tumor weight (g)
NS
k
4T1
Lung metastases count
Lung metastases count
**

Figure 4

a

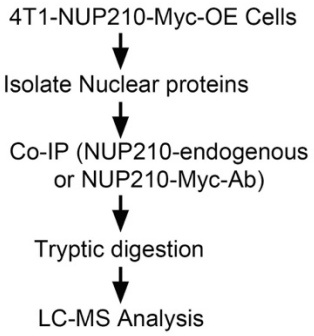

b

Peptides identified in LC-MS

Protein Name	NUP210-Endogenous		NUP210-Myc Tag	
	Rep-1	Rep-2	Rep-1	Rep-2
NUP210	116	93	80	64
Histone H3.1	5	11	1	5
RPL8	4	4	5	11
HMGB1		6	9	
ESRP1	1	5	2	4
RRP1B	4	2	5	2
NRROS	2	3	8	4
DGCR8	2	3	5	4
PRPF6	3	2	4	3
UTP14A	3	2	2	4

c

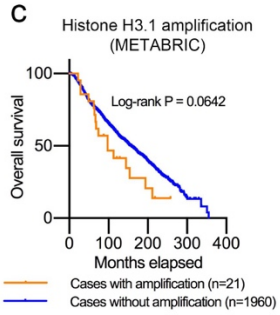

d

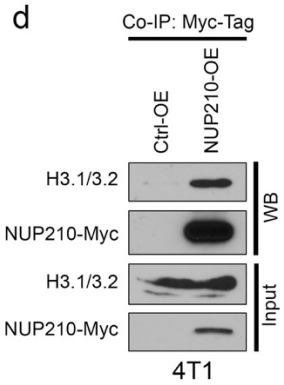

e

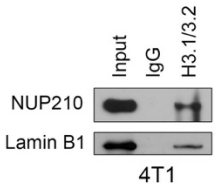

f

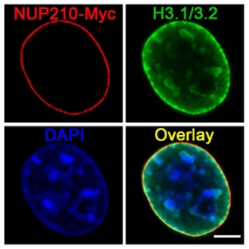

g

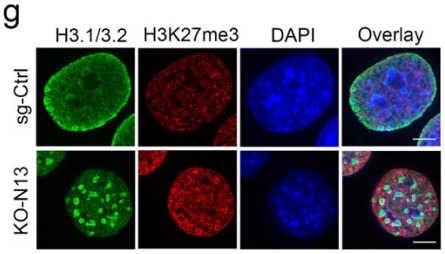

h

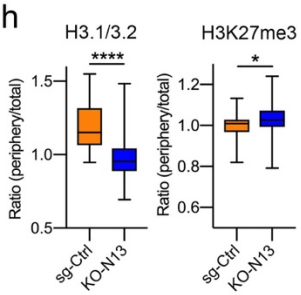

i

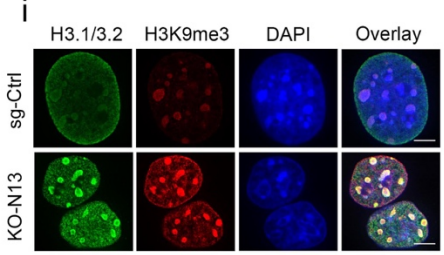

j

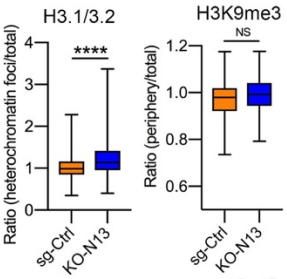

k

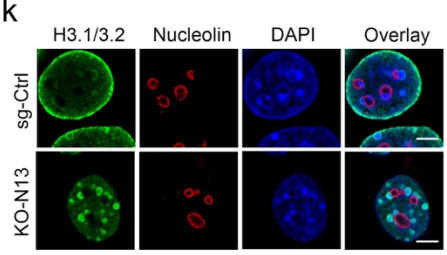

l

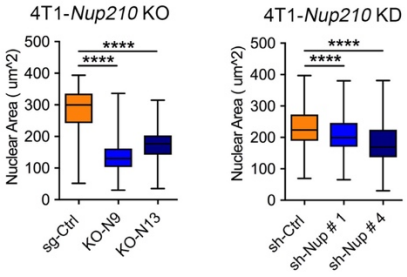

m

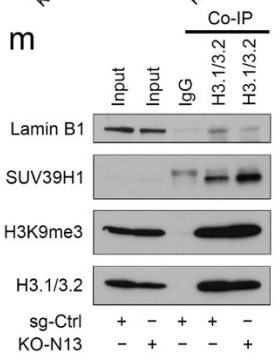

n

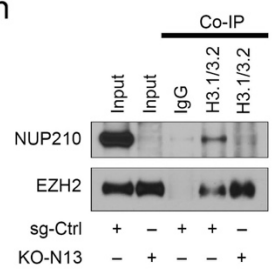

o

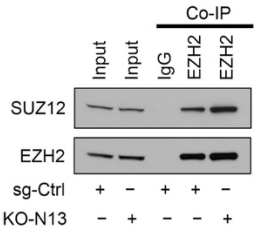

p

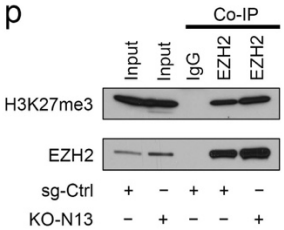

Figure 5

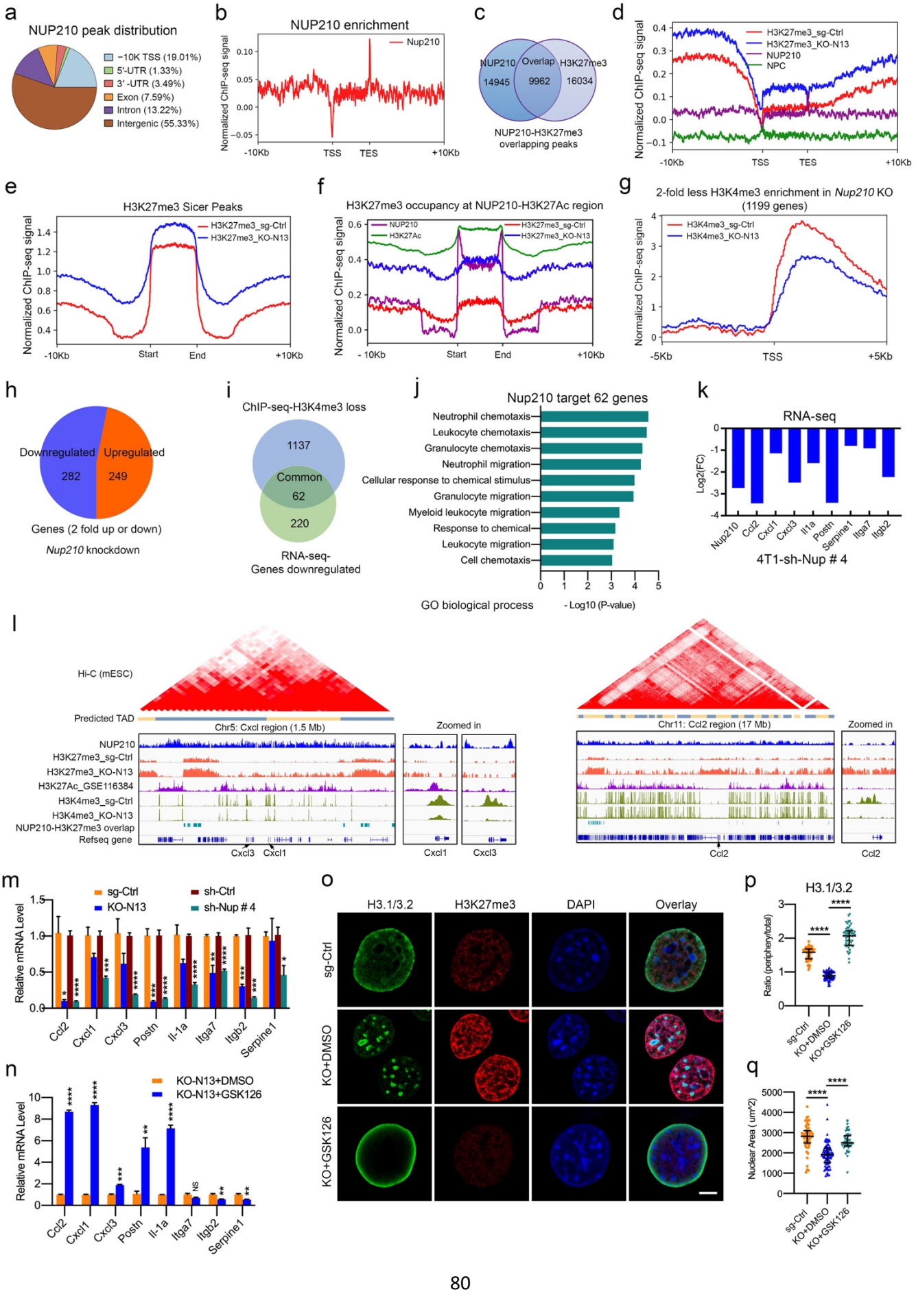
a
NUP210 peak distribution
−10K TSS (19.01%)
5′-UTR (1.33%)
3′ -UTR (3.49%)
Exon (7.59%)
Intron (13.22%)
Intergenic (55.33%)
b
NUP210 enrichment
Nup210
Normalized ChIP-seq signal
-10Kb
TSS
TES
+10Kb
c
NUP210
Overlap
H3K27me3
14945
9962
16034
NUP210-H3K27me3 overlapping peaks
d
H3K27me3_sg-Ctrl
H3K27me3_KO-N13
NUP210
NPC
Normalized ChIP-seq signal
-10Kb
TSS
TES
+10Kb
e
H3K27me3 Sicer Peaks
H3K27me3_sg-Ctrl
H3K27me3_KO-N13
Normalized ChIP-seq signal
-10Kb
Start
End
+10Kb
f
H3K27me3 occupancy at NUP210-H3K27Ac region
NUP210
H3K27Ac
H3K27me3_sg-Ctrl
H3K27me3_KO-N13
Normalized ChIP-seq signal
- 10Kb
Start
End
+10Kb
g
2-fold less H3K4me3 enrichment in Nup210 KO (1199 genes)
H3K4me3_sg-Ctrl
H3K4me3_KO-N13
Normalized ChIP-seq signal
-5Kb
TSS
+5Kb
h
Downregulated
Upregulated
282
249
Genes (2 fold up or down)
Nup210 knockdown
i
ChIP-seq-H3K4me3 loss
1137
Common
62
220
RNA-seq-
Genes downregulated
j
Nup210 target 62 genes
Neutrophil chemotaxis
Leukocyte chemotaxis
Granulocyte chemotaxis
Neutrophil migration
Cellular response to chemical stimulus
Granulocyte migration
Myeloid leukocyte migration
Response to chemical
Leukocyte migration
Cell chemotaxis
GO biological process
- Log10 (P-value)
k
RNA-seq
Log2(FC)
Nup210
Ccl2
Cxcl1
Cxcl3
Il1a
Postn
Serpine1
Itga7
Itgb2
4T1-sh-Nup # 4
l
Hi-C (mESC)
Predicted TAD
Chr5: Cxcl region (1.5 Mb)
Zoomed in
NUP210
H3K27me3_sg-Ctrl
H3K27me3_KO-N13
H3K27Ac_GSE116384
H3K4me3_sg-Ctrl
H3K4me3_KO-N13
NUP210-H3K27me3 overlap
Refseq gene
Cxcl3
Cxcl1
Cxcl1
Cxcl3
Chr11: Ccl2 region (17 Mb)
Zoomed in
Ccl2
Ccl2
m
sg-Ctrl
KO-N13
sh-Ctrl
sh-Nup # 4
Relative mRNA Level
Ccl2
Cxcl1
Cxcl3
Postn
Il-1a
Itga7
Itgb2
Serpine1
n
KO-N13+DMSO
KO-N13+GSK126
Relative mRNA Level
Ccl2
Cxcl1
Cxcl3
Postn
Il-1a
Itga7
Itgb2
Serpine1
o
H3.1/3.2
H3K27me3
DAPI
Overlay
sg-Ctrl
KO+DMSO
KO+GSK126
p
H3.1/3.2
Ratio (periphery/total)
sg-Ctrl
KO+DMSO
KO+GSK126
q
Nuclear Area (um^2)
sg-Ctrl
KO+DMSO
KO+GSK126

Figure 6

a

3D-DNA FISH analysis

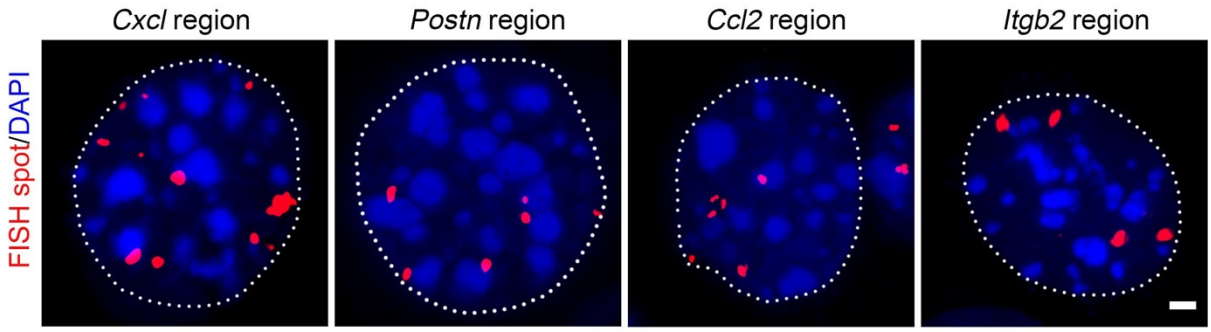

b

Relative position of FISH spots (Nuclear periphery vs centroid)

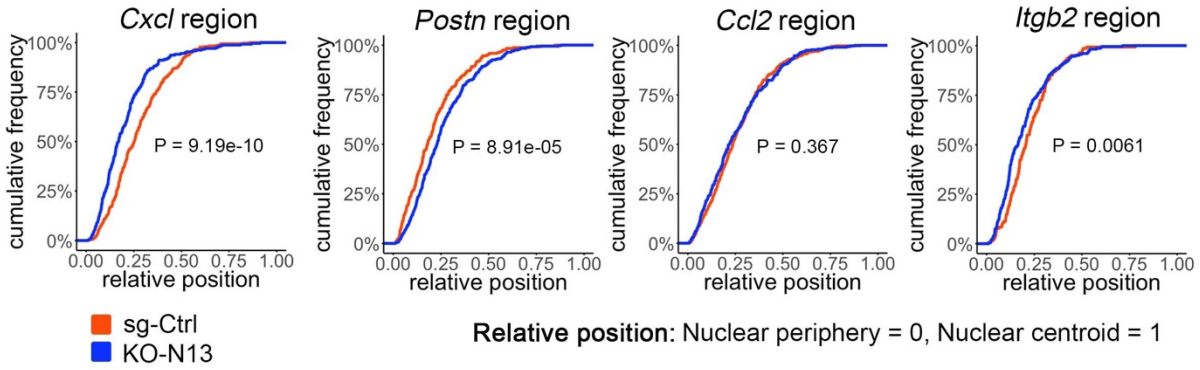

Relative position: Nuclear periphery = 0, Nuclear centroid = 1

c

Distance of FISH spots from heterochromatin foci

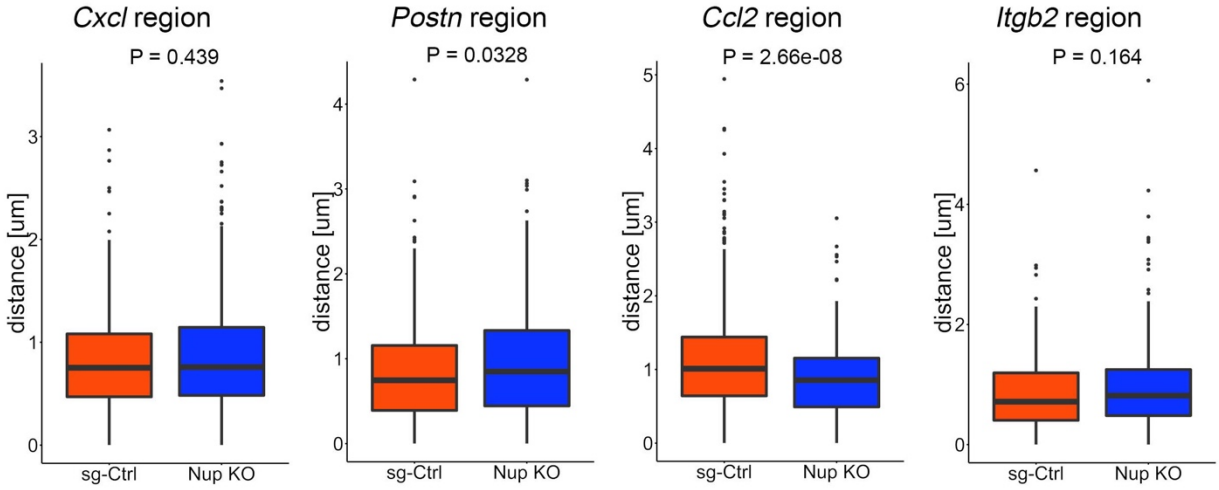

Figure 7

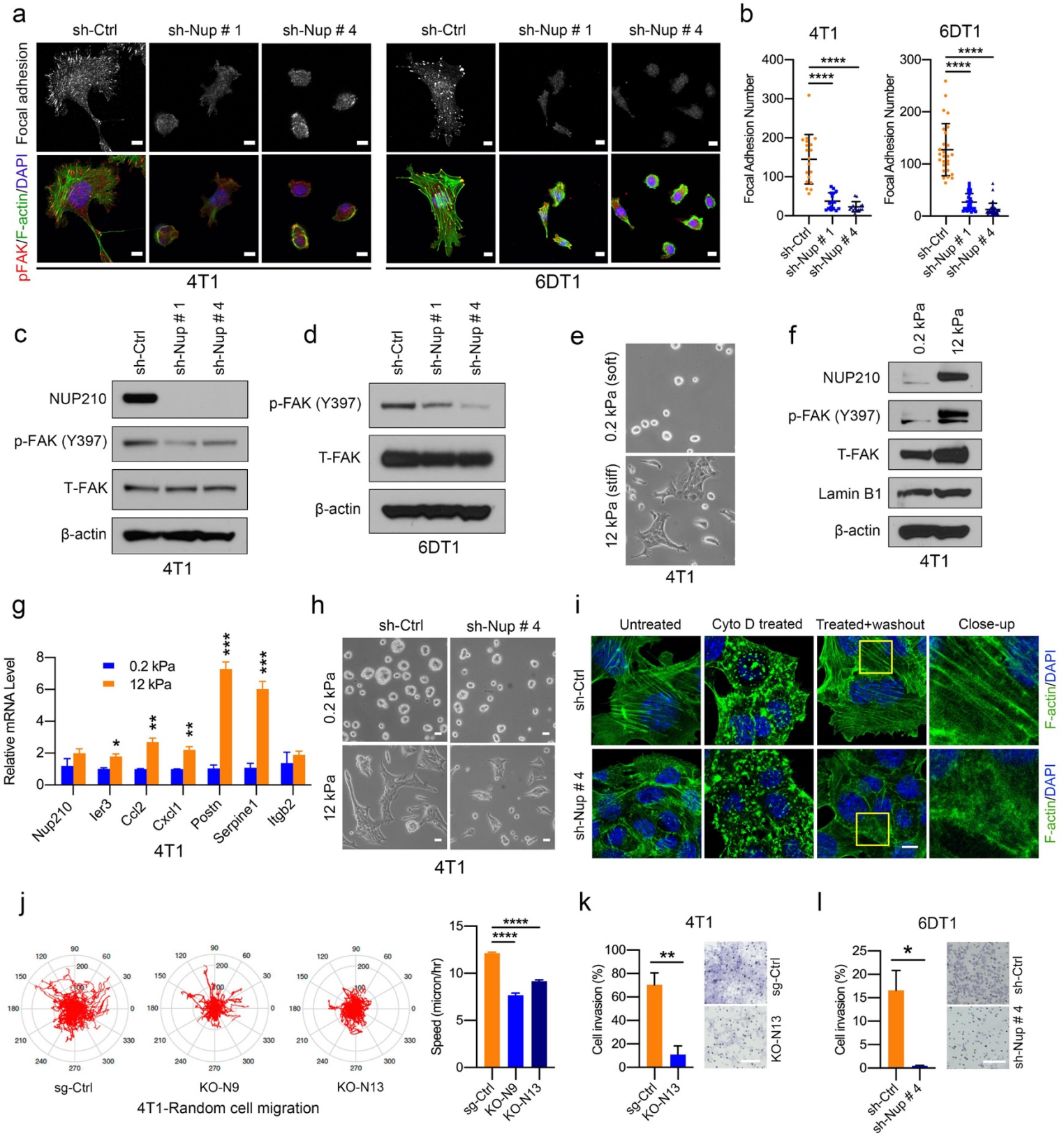
a
sh-Ctrl
sh-Nup # 1
sh-Nup # 4
Focal adhesion
pFAK/F-actin/DAPI
4T1
6DT1
b
4T1
6DT1
Focal Adhesion Number
****
c
NUP210
p-FAK (Y397)
T-FAK
β-actin
4T1
d
6DT1
e
0.2 kPa (soft)
12 kPa (stiff)
4T1
f
0.2 kPa
12 kPa
Lamin B1
g
Relative mRNA Level
0.2 kPa
12 kPa
Nup210
Ier3
Ccl2
Cxcl1
Postn
Serpine1
Itgb2
h
0.2 kPa
12 kPa
i
Untreated
Cyto D treated
Treated+washout
Close-up
F-actin/DAPI
j
sg-Ctrl
KO-N9
KO-N13
4T1-Random cell migration
Speed (micron/hr)
k
Cell invasion (%)
l

Figure 8

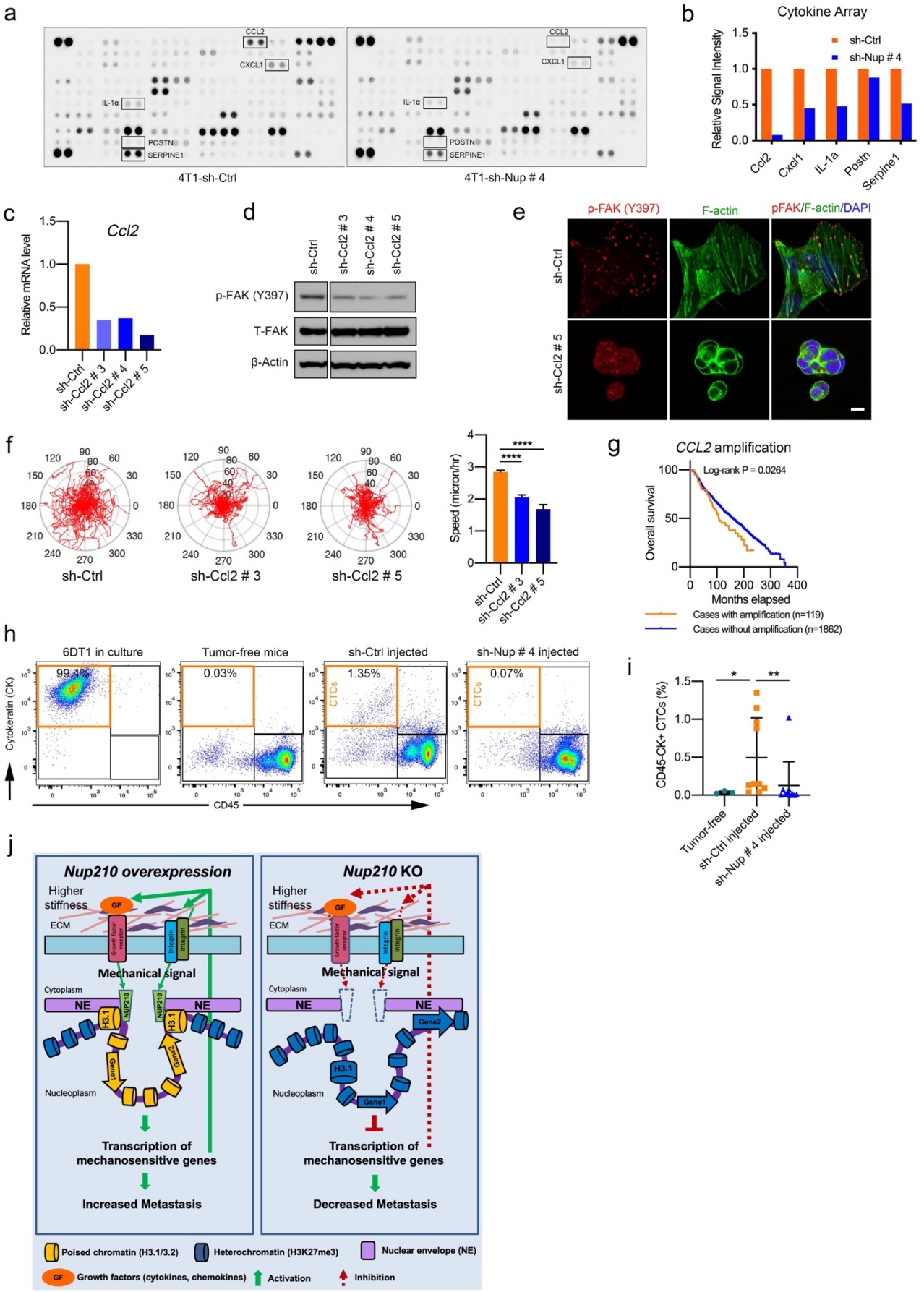
a
CCL2
CXCL1
IL-1α
POSTN
SERPINE1
4T1-sh-Ctrl
4T1-sh-Nup # 4
b
Cytokine Array
Relative Signal Intensity
sh-Ctrl
sh-Nup # 4
Ccl2
Cxcl1
IL-1a
Postn
Serpine1
c
Ccl2
Relative mRNA level
sh-Ctrl
sh-Ccl2 # 3
sh-Ccl2 # 4
sh-Ccl2 # 5
d
sh-Ctrl
sh-Ccl2 # 3
sh-Ccl2 # 4
sh-Ccl2 # 5
p-FAK (Y397)
T-FAK
β-Actin
e
p-FAK (Y397)
F-actin
pFAK/F-actin/DAPI
sh-Ctrl
sh-Ccl2 # 5
f
sh-Ctrl
sh-Ccl2 # 3
sh-Ccl2 # 5
Speed (micron/hr)
****
****
g
CCL2 amplification
Log-rank P = 0.0264
Overall survival
Months elapsed
Cases with amplification (n=119)
Cases without amplification (n=1862)
h
6DT1 in culture
Tumor-free mice
sh-Ctrl injected
sh-Nup # 4 injected
99.4%
0.03%
1.35%
0.07%
CTCs
Cytokeratin (CK)
CD45
i
CD45-CK+ CTCs (%)
*
**
Tumor-free
sh-Ctrl injected
sh-Nup # 4 injected
j
Nup210 overexpression
Higher stiffness
GF
ECM
Growth factor receptor
Integrin
Mechanical signal
Cytoplasm
NE
NUP210
H3.1
Gene1
Gene2
Nucleoplasm
Transcription of mechanosensitive genes
Increased Metastasis
Nup210 KO
Higher stiffness
GF
ECM
Mechanical signal
Cytoplasm
NE
Gene2
H3.1
Gene1
Nucleoplasm
Transcription of mechanosensitive genes
Decreased Metastasis
Poised chromatin (H3.1/3.2)
Heterochromatin (H3K27me3)
Nuclear envelope (NE)
GF
Growth factors (cytokines, chemokines)
Activation
Inhibition

Supplementary Figure 1

a

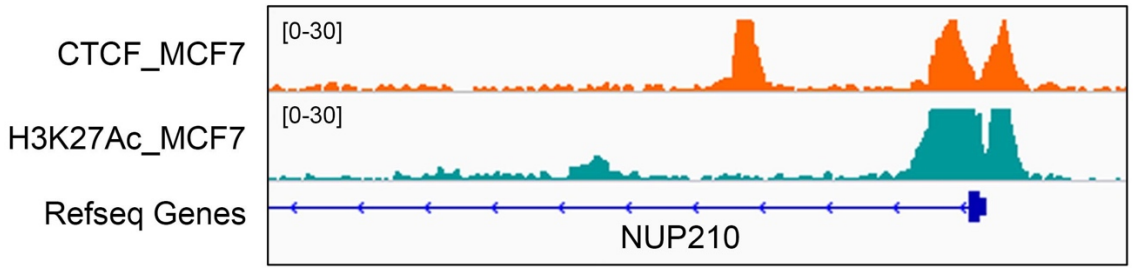

CTCF and H3K27Ac occupancy in Human *NUP210* promoter

Supplementary figure 2

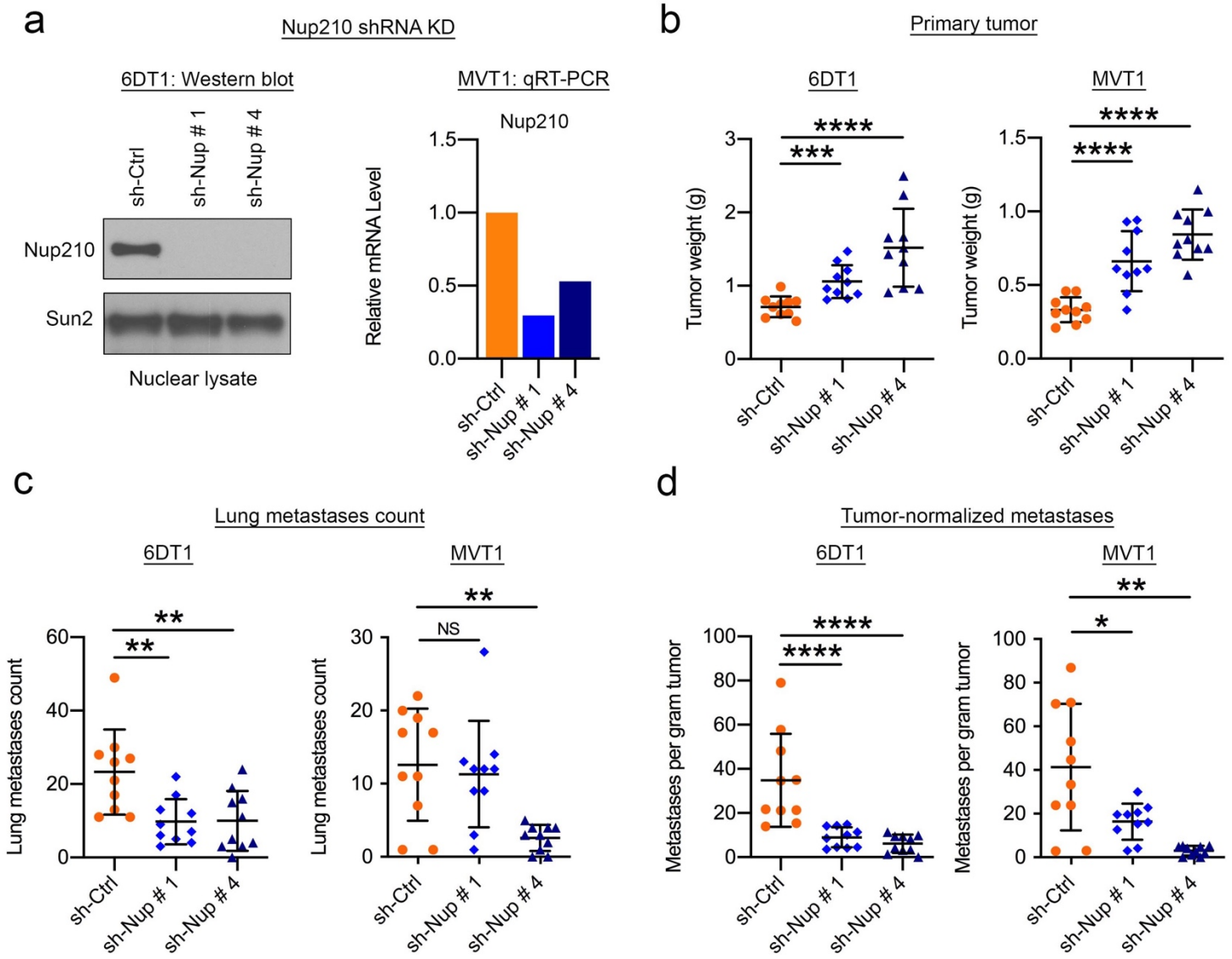

Supplementary figure 3

a

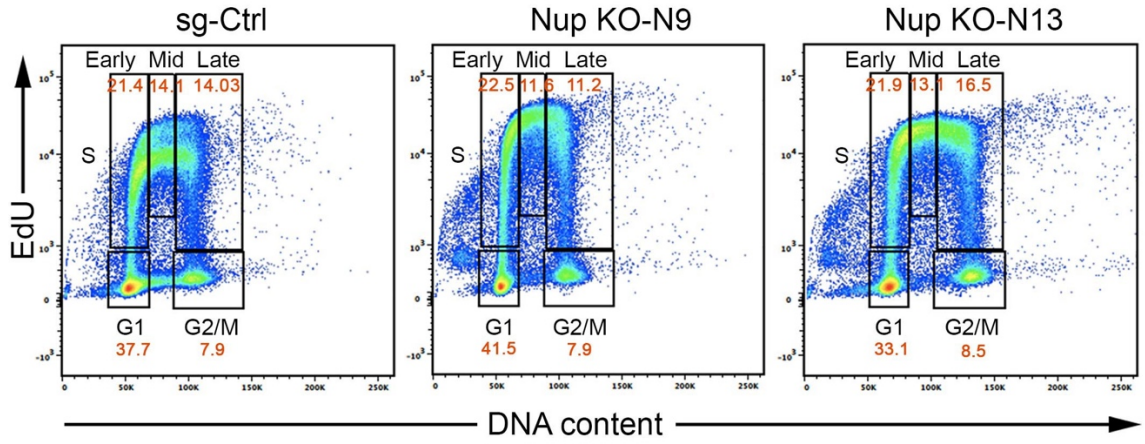

b

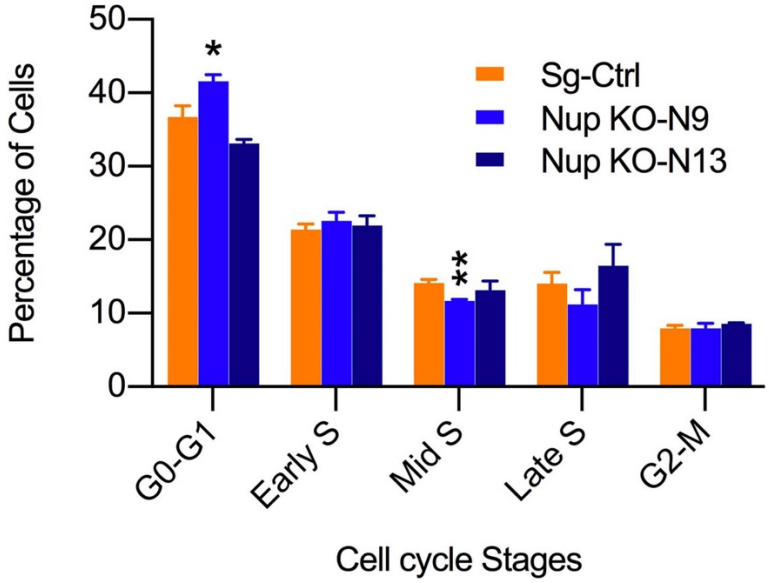

Supplementary figure 4

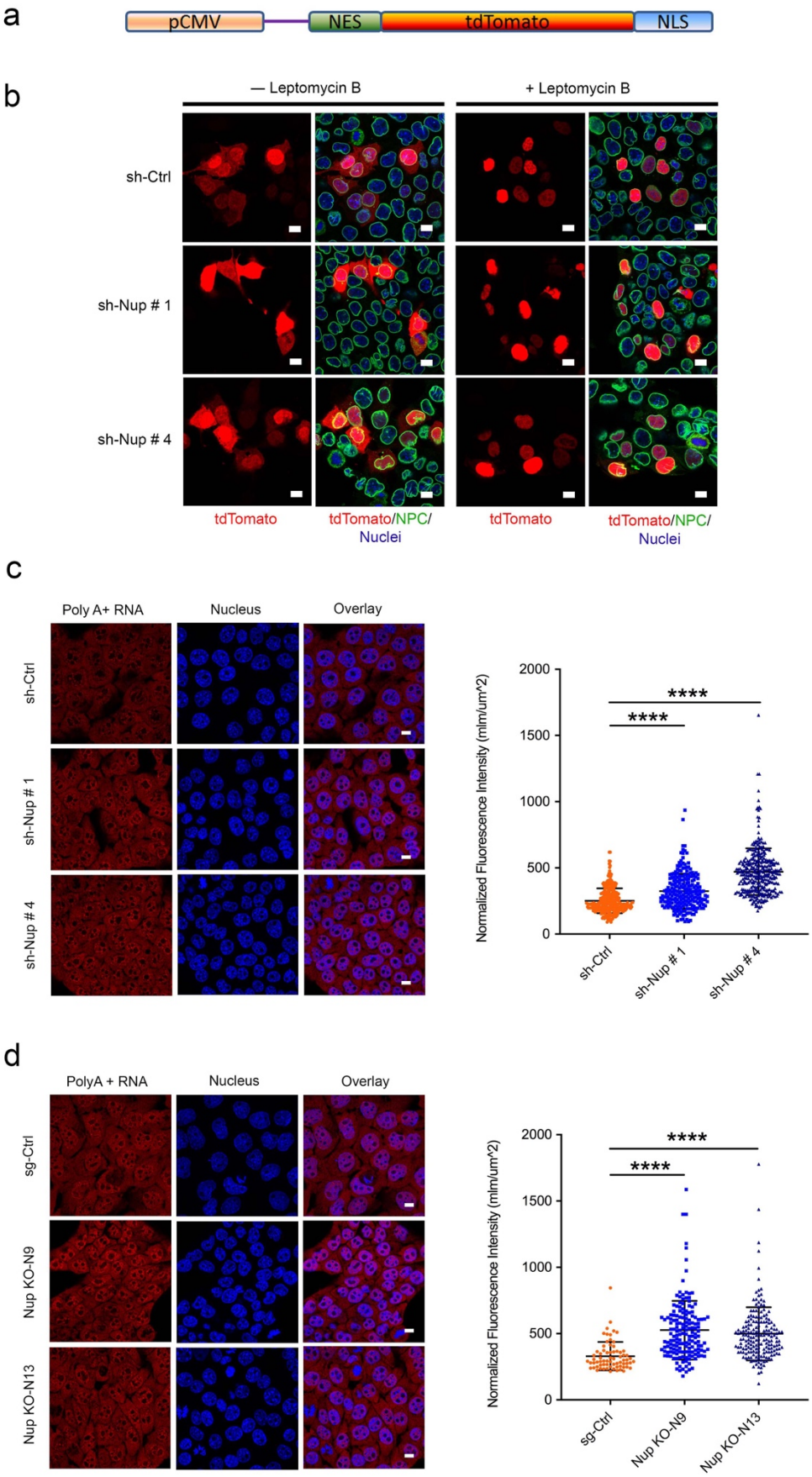
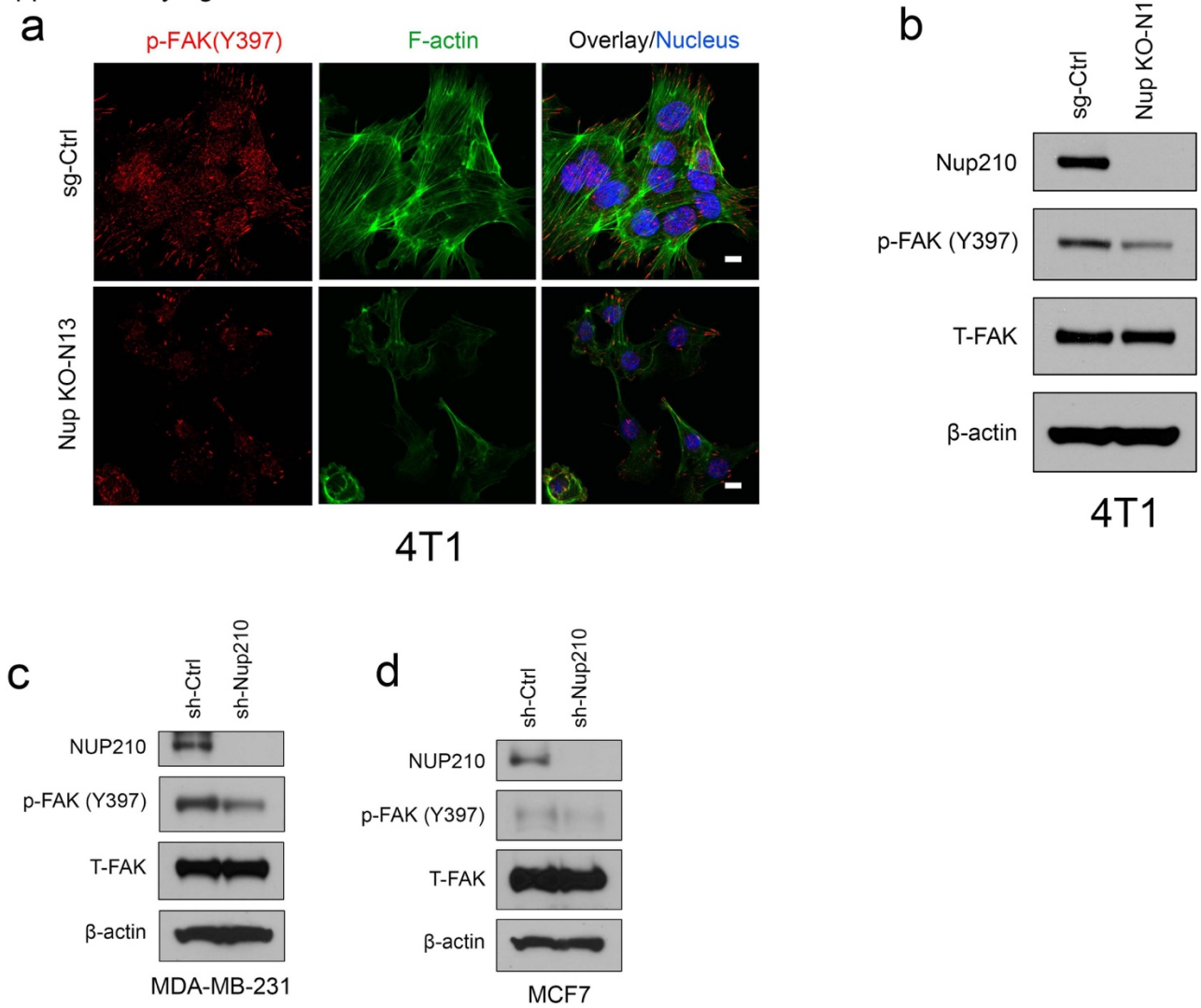
Supplementary figure 5